Computer simulation of blood flow in the human arm

by

Salil D. Balar

A Thesis Submitted to the
Graduate Faculty in Partial Fulfillment of the
Requirements for the Degree of
MASTER OF SCIENCE

Major: Biomedical Engineering

Iowa State University
Ames, Iowa

1985

TABLE OF CONTENTS

NOMENCLATURE

A	cross-sectional area
A_0	cross-sectional area at reference pressure p_0
A_1	area of obstructed arterial lumen
A_2	literature value of cross-sectional area at the distal end of the brachial artery
A_3	literature value of cross-sectional area at the proximal end of the radial artery
A_d	cross-sectional area at the distal end of the radial artery
A_m	Input value of cross-sectional area for the distal end of the brachial artery and proximal end of the radial artery
A_p	cross-sectional area at the proximal end of the brachial artery
a_0	wave speed
C_0^a	coefficient of polynomial
C_0^a	coefficient of polynomial
C_0	linear compliance term
C_1	nonlinear compliance term
C_{lumped}	lumped compliance
C_{total}	total arterial volumetric compliance
C_{tube}	arterial volumetric compliance

C_u	compliance per unit length
C_T	terminal compliance
D	diameter of the unobstructed lumen
D_1	diameter of the obstructed lumen
E	Young's modulus
h_0	arterial wall thickness
j^2	-1
K	the reflection coefficient
K_t	the turbulence coefficient
K_u	the inertial coefficient
K_v	the viscous coefficint
L	length of the stenosis
L_u	inertance per unit length
p	pressure
p_0	reference pressure, 95 mm Hg
Q	flow rate
R	peripheral resistance of the arm
$R_{T(distal)}$	peripheral resistance of the distal bed
$R_{T(ulnar)}$	peripheral resistance of the ulnar branch
t	time
V	volume of the entire artery
V_0	volume of the entire artery at reference pressure p_0

x	longitudinal coordinate
Z_0	characteristic impedance
Z_T	terminal impedance
α	frequency parameter
μ	viscosity of the fluid
ν	kinematic viscosity of the fluid
ω	heart frequency
ρ	density of the fluid
τ	shear stress
θ	phase angle

INTRODUCTION

Atherosclerosis is not commonly found in the brachial and radial arteries; hence, these arteries have not been studied as extensively as other arteries such as the coronary artery, carotid artery and femoral artery. However, the study of flow in the brachial and radial arteries may be useful for diagnostic purposes in many clinical situations. The heart pulse is usually measured from the radial artery, and blood pressure is measured in the brachial artery. Many investigators have measured parameters such as pulse wave velocity and compliance in these arteries (Fulton and McSwiney, 1925, Gribbin et al., 1976, Smulyan et al., 1983, Scarpello et al., 1980, Avolio et al., 1983, Simon et al., 1983, Randall et al., 1984). Others have studied how heart disease, aortic valve disease, hypertension, diabetes, hyperemia and hyperthyrodism are related to the nature of the waveform in the brachial or radial artery (Hancock and Abelmann, 1957, Kannel et al., 1981). The study of the brachial and radial arteries is of major clinical importance since arterial pressure is (values of systolic and diastolic pressures) conventionally measured from the brachial artery, and is used as a measure of the pressure in the proximal aorta, and the remaining arterial system. This value of blood pressure can be misleading, if we do not consider the differences in the nature of the pulse in the brachial artery under various conditions (O'Rourke, 1982). Blood pressure is measured to distinguish persons having hypertension and in 1979, 3.2 million

people in the United States had hypertensive conditions which caused a limitation of activity (U.S. Department of Health and Human Services, 1982, p. 29). Even though hypertension is not a immediate cause of death, there exist extensive evidence that hypertension is responsible for many other diseases such as stroke, heart disease etc. (Kannel et al., 1981).

In spite of the above clinical applications of the brachial and the radial arteries, there has been very few attempts to model these arteries. One reason for this is that a serious disease such as atherosclerosis is not prevalent in these arteries. It was decided to model the brachial and radial arteries, since the anatomy of these arteries is simple, and by studying the nature of the pressure and the flow waveforms in these arteries, it may be possible to use the waveforms to diagnose some common diseases such as heart disease and hypertension. It is possible to construct a computer model of the system using previously developed finite element programs (Weerapulli, 1986). This same program can also be modified to study other arteries such as the coronary arteries and the carotid artery.

An extensive literature survey was done to find suitable data for the brachial and radial arteries, while the system of differential equations cited by Raines et al. (1974) was used to describe the variation of flow and pressure in the arteries.

Brachial and Radial Arterial Pulses in Health and Disease

"There is in clinical medicine no physical sign more basic or important than the arterial pulse" (O'Rourke, 1970). This subject is of a prime interest. Many people have studied arterial pulses in various arteries such as the aorta, carotid, femoral, brachial, and radial. It is beyond the scope of this thesis to give a comprehensive literature survey which covers pulses in the carotid arteries and femoral arteries. Only some important studies highlighting the importance of the brachial and radial pulses in healthy and diseased arteries are discussed here.

The recording of the arterial pressure pulse by direct puncture of the brachial artery was considered to be a routine procedure in clinical cardiac physiology in the mid-fifties of this century (Hancock and Abelmann, 1957). Hancock and Abelmann (1957) attempted to diagnose aortic valve lesions from arterial pulse contours, which were scant and fragmentary at that time. The above work was done on normal subjects and various groups of patients with severe aortic stenosis, mild aortic stenosis, myocardial failure, aortic insufficiency, severe rheumatic mitral insufficiency without stenosis, anemia, and hypertension. A prolonged duration of systolic upstroke and an anarobic notch were found in most instances of severe aortic stenosis and frequently in patients with insignificant degrees of aortic stenosis as well as occasionally in normal subjects. In cases of aortic insufficiency, mitral insuffiency, anemia, hyperthyrodism

and exercise, characteristic but nondiagnostic changes in the pulse form were observed. Unfortunately, the brachial arterial tracings encountered in normal subjects vary considerably, and overlap to some extent the tracings associated with disorders of the circulation, and hence such tracings were difficult to interpret as a clinical diagnostic test. It was also noted that the brachial arterial pulse contour may serve to confirm a clinical diagnosis of aortic stenosis but in any individual patient yields no information as to the severity of the lesion.

Mason et al. (1964) computed first and second derivatives of the brachial arterial pressure pulse in normal subjects and in patients with idiopathic hypertrophic subaortic stenosis, discrete subvalvular subaortic stenosis, valvular aortic stenosis, combined aortic stenosis and regurgitation, and pure aortic regurgitation. This quantitation served as a useful diagnostic tool in separation of the various groups of patients. The analysis of the dp/dt and of d^2p/dt^2 of the brachial artery pressure pulse was proved to be a simple and reliable assessment of the nature and location of left ventricular outflow obstruction and helpful in the differentiation of valvular aortic stenosis, combined stenosis and regurgitation, and pure aortic regurgitation.

Gault et al. (1966) did a basic study on patterns of brachial arterial blood flow in conscious human subjects with and without cardiac dysfunction, which permitted the investigation of rapid, transient alterations in peripheral arterial blood flow not previously

accessible to measurement. An electromagnetic flowmeter was used to measure brachial arterial blood flow and recorded phasic flow patterns in subjects without significant left heart disease, as well as in patients having various cardiac lesions. Also investigated were the patterns of mean brachial arterial blood flow in the resting state, the instantaneous changes in the mean flow during local anesthesia and surgical exposure of the brachial artery, and the influence of reflex interventions on the brachial arterial flow. In interpreting the various reflex interventions described above, it was recognized that the complexity of the vascular bed served by the brachial artery influences greatly both the quantitative and directional changes in forearm vascular resistance (FVR). A delayed rise in systolic flow rate was observed in patients with aortic stenosis and an absence of dicrotic wave in patients with severe aortic regurgitation. These observations were helpful in distinguishing these patients from normal subjects.

Even though Ewy et al. (1969) worked mainly on the carotid pulse, they also determined a useful conclusion about the similar behavior of the brachial arterial pressure pulse. The indirect carotid pulse was characterized by a single systolic wave, a low dicrotic notch, and large dicrotic wave. The brachial arterial pressure pulse had a similar configuration with a shortened ejection time index. The presence of a marked dicrotic pulse in afebrile (without symptoms of fever) patients at rest may indicate severe functional impairment of the myocardium.

Hawker et al. (1974), O'Rourke et al. (1968) and O'Rourke (1970) found that in adults, amplification between the origin of the aorta and the proximal end of the brachial artery (which includes the aorta, subclavian artery and axillary artery) was less in patients with all types of aortic valve disease than in controls, whereas it had been previously shown that amplification in the descending aorta (which supplies blood to the abdomen and lower extremity) was not related to aortic valve disease. The explanation of this dissimilarity is that the lower harmonics are amplified more in the upper limbs, while the higher harmonics are amplified relatively more in the lower limbs. Since in an aortic stenosis most of the energy of the wave is in the lower harmonics, amplification in the brachial artery, but not in the descending aorta, might be expected.

Inagaki et al. (1976) studied the effects of treadmill exercise on the slope of the brachial arterial pulse wave along with other cardiac parameters, and these studies provide a baseline for analysis of patients with cardiovascular disease.

Millington and Record (1977) measured the radial arterial pulse under clinical conditions. In the literature review, it is stated that the method of pressure recordings of the radial pulse is useful in detecting arterial diseases, and the time derivative of pressure could be a sensitive indicator of cardiac ejection performance and valve function.

Barnes et al. (1974) mentioned that the measurement of forearm blood pressure compared to arm pressure is a useful quantification of

the presence and hemodynamic significance of brachial artery obstruction following cardiac catheterization.

Karwash et al. (1979) were interested in the disease diagnosis from arterial pressure waveforms, and stated, "Currently, our most common procedure, partly because of simplicity, is to simultaneously record the pressure profiles from the brachial and radial arteries." A comparison of representative tracings of waveforms taken from a typical young healthy male and from an elderly healthy male, showed the striking difference in the prominence of the dicrotic wave.

Bennett et al. (1980) noninvasively measured brachial artery peak velocity (BAPV) as an index of cardiac performance in normal subjects and in patients with acute myocardial infarction (AMI). BAPV in patients with AMI was significantly less. BAPV in patients with acute AMI who died was the least, and was significantly less than the AMI patients who had survived.

Kannel et al. (1981) concluded that the prevalence of isolated systolic hypertension increased with age and with the degree of blunting of the dicrotic notch in the pulse wave. Hypertensive subjects experienced more risk of strokes compared to normal subjects. A comparison of pulse-wave recordings in subjects with hypertension, arteriosclerosis, and diabetes, concludes that the appearance of the dicrotic notch was the most important diagnostic feature of the peripheral pulse wave.

In contrast to above studies, Giuliani and Gould (1969) saw a risk in evaluating the valvular aortic stenosis from the brachial

arterial pressure. A study was performed on two patients with severe aortic stenosis, both with cardiac catheterization and peripheral arterial pulse pressures. It was observed that the ejection time, first derivative and upstroke time of brachial artery pressure were compatible with severe aortic stenosis, but in the case of mild stenosis only the cardiac catheterization gave a reliable estimate in diagnosing the aortic stenosis.

In spite of the above exception, numerous current studies have proved the importance of the brachial and radial arterial pulses in the clinical diagnosis of arterial diseases. Moreover, due to the simplicity of the anatomy of these arteries and the convenience of measuring pulses from these arteries, these arteries may be possibly adopted for a routine procedure in the diagnosis of arterial diseases especially near the heart. In addition to the development of sophisticated and reliable instruments for noninvasive recording of waveforms, use of computer-generated waveforms and computer-based data processing can certainly give a better insight into the interpretation of the waveforms.

History of Hemodynamics and Development of Arterial Models

In the eighteenth century, Stephen Hales contributed invaluably to the fascinating field of arterial dynamics and certainly deserved the title 'The Father of Hemodynamics' (quoted by McDonald, 1974). He was the first person who measured blood pressure in the horse. He also

introduced the concept of the peripheral resistance. He showed that the distensible properties of the arteries, forming a Windkessel (elastic reservoir) during ventricular systole, are responsible for the smooth change of pulsatile flow in the arteries into the steady flow in veins (McDonald, 1974).

After Hale's work, Euler's equations of fluid motion, Bernoulli's Law of energy, Poiseuille's law of viscous flow through a tube, the Navier-Stokes equations, Thomas Young's elastic modulus, Fourier series for the analysis of periodic functions, and the Moens-Korteweg equation of pressure pulse wave velocity were remarkable contributions (before the twentieth century) to the field of fluid dynamics and to modern hemodynamics.

In the late nineteenth and earlier twentieth century, Frank's work on the Windkessel model based on time-domain considerations was considered to be important (Westerhof et al., 1977). After Womersley (1955) and McDonald (1955) used Fourier series for the analysis of the pressure and flow waveforms, the Windkessel models of elastic reservoirs were less frequently used, and the approach to arterial system entered the frequency domain. Some of Womersley's mathematical analysis regarding pressure-flow relationships in arteries was tested experimentally by McDonald on the femoral artery of dog, while some of McDonald's experimental results were checked mathematically by Womersley (for example, McDonald, 1952, 1955; Helps and McDonald, 1953, 1954; Womersley, 1954, 1955). This kind of close agreement on analytical and experimental results started a new era in hemodynamics.

In addition, availability of good flowmeters accelerated this kind of trend-setting work, and many investigators started testing theoretical work by actually measuring the blood flow in arteries in vivo.

Measurements of Hemodynamic Parameters and Modeling Approach in Brachial and Radial Arteries

Measurement of pressure and its physiological significance

As mentioned earlier, pressure measurements in the brachial artery became clinically important because values of systolic and diastolic pressures obtained in the brachial artery were usually represented as those values in the proximal aorta and in the rest of the system. Kroeker and Wood (1955, 1956) studied extensively the pressure transmission from central to peripheral arteries by simultaneously recording central and peripheral arterial pressure pulses at many sites in the steady state under varying physiological conditions as well as during rapid alterations in the cardiovascular status of normal persons induced by the Valsalva maneuver or a prolonged expiration. It was found that amplification of the pressure pulse between the aortic arch and brachial artery under basal conditions averaged 31 percent, while amplification to the radial artery averaged 46 percent, and to the femoral artery averaged 39 percent. Their results were supported later by O'Rourke (1970), who found average amplification of 18 percent to the brachial artery while amplification to the iliac artery averaged 24 percent (in a similar

study, but on patients undergoing cardiac catheterization). Kroeker and Wood's (1955, 1956) measured values indicated definite increase in systolic pressure from the brachial to radial arteries in the same arm. Even though the increase was small, it was quite noticeable.

O'Rourke (1982) reported the physiological significance and factors affecting the pulse transmission to the brachial artery by discussing the results of Kroeker and Wood (1955, 1956) and O'Rourke (1970). O'Rourke (1970) did not find any consistent relationship between age and brachial amplification in contrast to the definite relationship previously shown between age and femoral amplification. Both O'Rourke (1970) and Kroeker and Wood (1955, 1956) agreed that brachial amplification was remarkably dependent on the duration of ventricular systole. The brachial amplification was decreased when systole was lengthened as in aortic valve disease, and increased when systole was shortened as by prolonged expiration, head-up tilt and during Valsalva's maneuver (an increase of intrapulmonic pressure by forcible exhalation against the closed glottis). The amplification of the pulse pressure to the radial artery also increased up to 200 percent during Valsalva maneuver. The brachial arterial pulse also increased in the leg exercise when the systole was shortened. The main reason for this increase is the change in ejection pattern and not the alteration in properties of arteries in the upper limb (O'Rourke, 1970). In support of earlier work done by Rowell in 1968, O'Rourke (1982) explained that similar to the femoral artery, brachial amplification is dependent on wave reflection in the peripheral

vascular bed, and almost disappears when vasodilation is induced in the upper limb. Kroeker and Wood (1955, 1956) explained this increase in amplification of the pressure pulse with decreased ventricular ejection period on the basis of resonance stating that when the frequency of the ventricular ejection (driving function) corresponds to the resonant frequency of the arterial system in the upper limb, the apparent exaggeration of wave reflection occurs.

Interpretation of directly recorded brachial artery pressure waves involves pressure pulse transmission to the brachial artery. O'Rourke (1982) clearly explained that when the duration of systole is shortened or resonant frequency of the whole arterial system or of specific vascular segments is decreased (as when blood pressure, and so, wave velocity, are decreased), brachial artery tracings may give a falsely high measure of systolic pressure and a falsely low measure of diastolic pressure in the ascending aorta and throughout the arterial system. However, these differences may be remarkably altered if shortened systole and hypotension are combined, as in clinical shock. So, under clinical conditions these differences should be measured in the proximal aorta.

One of the earliest studies regarding the physiological relationships of arterial pressures was done by Hamilton et al. (1936). It was found that the systolic pressures progressively increase as we go from the femoral and then on down to the foot (dorsalis pedis); however, the diastolic pressures are nearly equal. The physical factors behind the increase in systolic pressure, as the

pulse wave approaches the periphery, seem to be in the lower limbs and abdominal aorta to a greater extent than in the arteries of the arm. Later on Kroeker and Wood (1955, 1956) and O'Rourke (1970) found the correct estimate for amplifications of pulse pressure in the femoral, brachial and radial arteries (which was mentioned earlier in this thesis).

It was demonstrated later (Doupe et al., 1939) that the systolic arterial pressure in the extremities may show considerable variations as the result of local vasomotor changes, and such variations are independent of alterations in systemic pressure (in central arteries). Alterations in the blood flow in the extremities are responsible for these phenomena. Measurements were taken of arterial pressure in the upper arm and forearm by the ordinary ausculatory method using a mercury manometer. Gaskell and Krisman (1958) found the brachial to digital pressure gradient greater in the hypertensive patients than that in the normal subjects in different vasomotor states by using the clinical ausculatory technique. Wallace and Stead (1959) found a decrease in pressure in the radial artery during reactive hyperemia in normal subjects. Approximately 30 per cent of the energy of pressure may be lost between the aorta and the radial artery, when the arterial bed between the aorta and radial artery offers an appreciable resistance to flow. The effect was more pronounced in patients with hypertension.

Kato et al. (1977) and Nakayama and Azuma (1977) measured digital arterial systolic, diastolic and mean blood pressures. Nakayama also

measured digital arterial compliance. Even though the present thesis is not related to the digital artery, the above studies can be helpful in the future extension of the arm arterial model to include the digital arteries. Another aspect of the arm-models is the study of the effects of external pressure on arm arterial pressure (Foley and Greenberg, 1969, Caro et al., 1968). One controversial subject regarding pressure measurement is the relationship between directly and indirectly measured brachial pressures. Even though Rastelli et al. (1968) reported that an indirect systolic pressure is lower than the direct level, and an indirect diastolic pressure is equal to or higher than the direct level, there is no known definite relationship between directly and indirectly recorded brachial artery pressure and there is far more variation in this relationship under basal condition (and more so under abnormal conditions) than most are aware of (Floras et al., 1981). This is due to the fact that the Korotkov sounds do not accurately identify systolic and diastolic pressures. The diastolic pressure varies so much that there is no internationally accepted standard for determining diastolic pressure, with some taking this to be cuff pressure at muffling of sound (phase 4) and some at disappearance of sound (phase 5) (O'Rourke, 1982). O'Rourke considered this topic of directly and indirectly measured arterial pressure as uncomfortable but important. In his words, the variable relationship between indirectly and directly recorded brachial artery pressure, and between directly recorded brachial artery pressure and aortic pressure underlines the importance of direct central aortic

pressure monitoring under such conditions as cardiogenic shock, where cardiac function must be assessed accurately, and intra-aortic balloon pumping timed correctly.

Measurement of flow and its physiological significance

Even though good flowmeters were only available in the market by the 1960s, earlier attempts were made to measure blood flow. Kerslake (1949) used his own previously developed automatic blood-flow recorder to record forearm blood flow at frequent and regular intervals. This study was primarily meant for observing changes in forearm blood flow occurring immediately after the application of an arterial occlusion cuff to the wrist of the subjects. Andres et al. (1954) measured forearm blood flow of man by continuous injection of solution of Evans blue dye. But in none of the above studies, was the blood flow through the brachial artery measured. Recently, Levenson et al. (1981) and Safar et al. (1981) measured blood flow in the brachial artery as well as the diameter and blood flow velocity. A pulsed doppler velocity meter was used with an adjustable range-gated time system and a double transducer probe for these determinations. The apparatus provided an accurate noninvasive method. Safar et al. (1981) monitored the hypertensive patients for similar measurements, and demonstrated that the diameter of the brachial artery increased significantly in sustained essential hypertension, and suggested that, with the chronic elevation of blood pressure, the

large arteries dilate excessively, contributing to the maintenance of arterial blood flow within normal ranges.

Estimation of compliance and its physiological significance

Recently many people have become interested in estimating the brachial arterial compliance, as it is suspected to be associated with various physiological factors and hemodynamic parameters. In one of the recent studies, Simon et al. (1983) determined forearm arterial compliance in normal and hypertensive men from simultaneous pressure and flow measurements in the brachial artery, using a pulsed doppler device and a first-order arterial model during diastole. Some important conclusions are: (1) The reduced forearm arterial compliance was associated with a significant increase in brachial artery diameter, (2) The reduced forearm compliance in hypertension is independent of blood pressure, but may reflect adaptive changes in the walls of the large arteries. Avolio et al. (1983) studied the effects of aging on changing arterial compliance while studying a northern Chinese urban community, and concluded that aging and not concomitant atherosclerosis is the dominant factor associated with reduced arterial compliance. In the literature review (Avolio et al., 1983), it was mentioned that the arterial pulse wave velocity is directly related to arterial wall stiffness, and since the pulse wave velocity increases with age, arterial wall stiffness also increases, and compliance decreases. The conclusion was derived by measuring the

aortic pulse wave velocity between the aortic arch and femoral artery, between the femoral artery and dorsalis pedis, and between the brachial and radial arteries. Randall et al. (1984) were curious about the effect of systemic compliance in the genesis of essential hypertension, but ultimately concluded that changes in arterial compliance alone cannot explain isolated systolic hypertension. Reduction of compliance was found to increase in systolic pressure and decrease in diastolic pressure, but there was no significant change in the mean pressure; however, cardiac output was reduced. It was pointed out that decreased compliance mainly caused changes in the low frequency range of the input impedence. Fitchett (1984) considered the forearm compliance as a possible useful indicator of the effect of physiological and pharmacological interventions on the distensible properties of arteries.

Measurement of pulse wave velocity and pulse wave transit time and their physiological significance

For a number of years, the pulse wave velocity has been studied extensively, and there are many studies related to both pulse wave velocity and pulse transit time in arm arteries. About sixty years ago, Fulton and McSwiney (1925) measured the pulse wave velocity in the brachial and radial arteries, and the pulse wave velocity was found to be always lower in the brachial than in the radial artery, but this change was not related with blood-pressure. Just a decade

ago, the pulse wave velocity was monitored along an arm artery to detect changes in mean blood pressure, but not to the absolute pressure (Gribben et al., 1976). Three years later, Obrist et al. (1979) related pulse transit time to systolic pressure (and also to myocardial sympathetic excitation), but failed to relate the pulse transit time to diastolic pressure. Two years later, Geddes et al. (1981) showed pulse transit time as an indicator of arterial diastolic blood pressure. A decrease in pulse arrival and transit time with an increase in diastolic blood pressure was found. They also reported a nonlinear relationship between pulse transit time and diastolic pressure, and a linear relationship between pulse wave velocity and diastolic pressure.

Apart from blood pressure, the pulse wave velocity was also studied for different purposes. The direct measurement of brachial to radial pulse wave velocity was used to calculate volume distensibility of forearm arteries, which eliminated arterial blood pressure as a variable as it strongly affects arterial distensibility (Smulyan et al., 1983). Comparison of normal subjects, to diabetic patients showed a significant increase in pulse wave velocity in the lower limbs, but no significant difference in pulse wave velocity in the upper limbs (Scarpello et al., 1980).

In the literature review, Scarpello et al. (1980) mentioned that the pulse wave velocity of the pressure and flow waves produced during ventricular ejection is a sensitive indicator of the physical properties of the arterial wall, and hence measurements of pulse wave

velocity may be used to determine changes in the condition of the arteries which occur as a result of vascular disease. The literature reviewed by Avolio et al. (1983) also reported that the pulse wave velocity is directly related to arterial wall stiffness and to wall thickness. Also it was noted that the characteristic impedance of an artery is directly related to regional arterial pulse wave velocity. It was concluded that the pulse wave velocity is directly related to change in arterial compliance, and a high correlation of pulse wave velocity with high prevalence of hypertension was found. The relationship of pulse wave velocity with age and arterial compliance was used to strongly argue against atherosclerosis as an important factor influencing arterial distensibility while the pulse wave velocity gives valuable information on arterial distensibility. Even though the pulse wave velocity can be measured noninvasively, there exists a drawback in that for accurate noninvasive determination it must be measured over a long length of the arterial system. Thus, the pulse wave velocity gives information on the properties of the whole vascular segment, whereas characteristic impedance gives information on the properties at the point of measurement.

Models of arm arteries

Many investigators have included the brachial and radial arteries in their models of the entire arterial tree (Noordergraf et al., 1963, Westerhof et al., 1969, Avolio et al., 1980). Others have measured

hemodynamic parameters such as pressure, flow, compliance, pulse wave velocity etc., in the brachial and radial arteries (as mentioned earlier). There are very few attempts to model only the brachial and radial arteries and to interpret various hemodynamic parameters. One such attempt was done by Wesseling (1973). A simplified, lumped, linear analogue-computer model was constructed of the arm arteries using simultaneously recorded pulsewaves from the brachial (input signals) and radial (comparison signals) arteries. A parameter estimation technique was used to obtain various hemodynamic parameters such as the arterial internal radius, arterial compliance and the magnitude of the amplification effect of the pulsewave with reasonably good results. However, values for peripheral resistance were consistently underestimated, as their model lacked viscous damping. Simon et al. (1983) constructed a first-order arterial model of the brachial artery, and estimated fairly accurate values of forearm arterial compliance and resistance based on measured values of pressure, diameter, flow velocity and volumetric blood flow.

In the above two models, nonlinearities are avoided. None of these models have interpreted pressure and flow waveforms using Fourier analysis, nor have they used the basic equations of fluid dynamics such as the continuity equation and momentum equations. These principles were used by many people to develop equations governing blood flow in other arteries of the body (for example, Raines et al., 1973, Porenta, 1982). Thus, there was a need to develop an arm arterial model by using the above approach to study the various

hemodynamic parameters such as pressure, velocity, flow, compliance and resistance. One such model has been prepared very recently (Clark et al., 1985), where the upper extremity arterial flow simulation representing main arteries from heart to digits has been modeled. Another model was also prepared which involves both upper extremities in the two arm model. A finite-difference scheme was used to solve the equations, and pressure and flow waveforms of normal and stenosed arteries of the arm are presented in three dimensional plots. In the present study, an arm arterial model has been prepared, which is different from that of Clark et al.'s (1985). Here, the finite element method is used, and the model is able to give pressure and flow waves at numerous intermediate points. The model may be helpful in studying the effect of mild and severe stenoses on pressure and flow values, and it can be used to study the effects of changing compliances and resistances on flow and pressure and in analyzing pressure and flow waveforms of patients having different heart diseases. Study of a simple model like this may give a better insight into the similar behavior of flow characteristics in more complicated models of vessels such as the carotid and coronary arteries.

MATHEMATICAL MODEL AND METHODOLOGY

Governing Equations

It has been shown by Raines et al. (1974) that the one-dimensional unsteady flow equations for incompressible fluids can be used to satisfactorily describe pulsatile flow in flexible tubes. The continuity equation is

$$\frac{\partial Q}{\partial x} + \frac{\partial A}{\partial t} = 0 \tag{1}$$

where Q is the flow rate, A the lumen area, x the longitudinal coordinate along the vessel, and t is time.

The momentum equation is

$$\frac{\partial Q}{\partial t} + \frac{\partial}{\partial x}(Q^2/A) = -\frac{A}{\rho}\frac{\partial p}{\partial x} + \frac{\tau \pi D}{\rho} \tag{2}$$

where τ is the shearing stress at the vessel wall.

The system is completed by specifying an equation of state relating the lumen area and the pressure. For this present study, this equation was assumed to be of the form

$$A(p,x) = A_0(p_0,x)\,(1 + C_0^a\,(p-p_0) + C_1^a\,(p-p_0)^2) \tag{3}$$

where A_0 is the lumen area at pressure p_0, and the coefficients of the polynomial C_0^a and C_1^a can be represented as follows:

$$C_0^a = \frac{1}{\rho a_0^2}$$

and

$$C_1^a = \frac{1}{\rho a_0^4}$$

where a_0 is the wave speed in the tube.

Stenosis

The simulation of a stenosis in an artery is based on the following relationship established by Young and Tsai (1973):

$$A_0 \frac{\Delta p}{\rho L} = (K_v) \frac{\mu}{DL\rho} Q + (K_t/2A_0) [(A_0/A_1) - 1]^2 \frac{Q|Q|}{L} + (K_u)\frac{\partial Q}{\partial t} \quad (4)$$

and

$$K_v = 32 [(0.83 L + 1.64 D_1)/D] (A_0/A_1)^2$$

where Δp is the pressure drop across the stenosis. The parameters A_0, D and A_1, D_1, are the areas and diameters of the unobstructed and obstructed arterial lumen, respectively, and L is the length of the stenosis. The viscous coefficient K_v, the turbulence coefficient K_t and the inertial coefficient K_u are experimental quantities and were originally determined to give the best fit of the data for the model. These coefficients generally depend on the stenosis geometry and the frequency parameter $\alpha = (D/2)\sqrt{\omega/\nu}$, where D is the lumen diameter, ν is the kinematic viscosity and ω is the fundamental frequency (or heart frequency) of the pulsatile flow.

In the present model, K_t and K_u were assigned the values 1.5 and 1.2. A detailed discussion of various hemodynamic factors pertaining to blood flow in stenosed arteries is given in Young (1979).

Boundary Conditions

A pressure waveform for the normal brachial artery from Mason et al. (1964) was used as the proximal boundary condition for the model for the control case. Similarly, for the case of hypertension, a pressure waveform from Simon et al. (1983) was used, while for the case of AS (valvular aortic stenosis), AI (pure aortic regurgitation) and AS/AI (combined valvular aortic stenosis and regurgitation), pressure waveforms from Mason et al. (1964), were used as the proximal boundary condition for the model. A pressure waveform is chosen for the proximal boundary condition considering Porenta's (1982) argument that the pressure waveform is probably less affected than the flow waveform by changes in the flow situations downstream from the proximal end of the brachial artery.

The distal boundary condition at the end of the arterial section was determined on the basis of Raines et al.'s (1974) study. It was decided to truncate the artery at the point before the distal bed begins, and to replace the distal bed by a lumped resistance. This makes the model much simpler by excluding details of small arteries, arterioles and capillaries in the model. In order to account for the distensibility of the distal bed, the model is terminated at the truncation by a lumped compliance C_T placed between two lumped resistances R_1 and R_2. The network formed by this system of lumped end condition is analogous to an electrical network (as shown in Figure 1), and the complex load impedance (equivalent to the terminal

impedance in the arterial model) of this electrical circuit is given by

$$Z_T = R_1 + \frac{R_2 \ (1-jR_2C_T \ \omega)}{1 + R_2^2 \ C_T^2 \ \omega^2} \tag{5}$$

where the sum of the two resistances R_1 and R_2 is taken to be the terminal resistance R_T. Also, ω is the heart frequency and $j^2 = -1$.

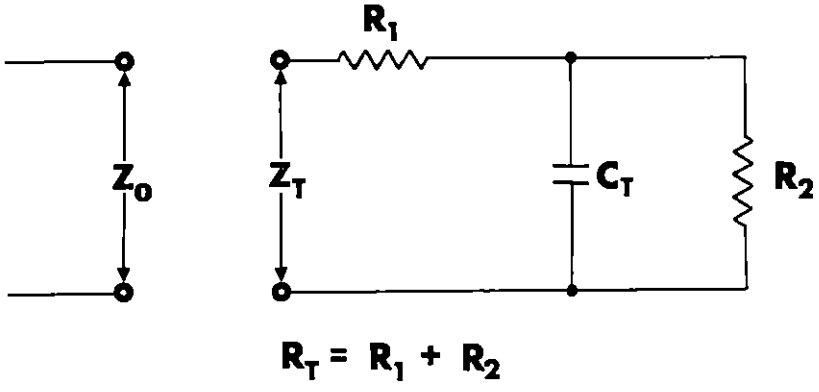

FIGURE 1. Electric analog of the distal boundary condition

The same principle is adopted in the present model, and the peripheral beds of the ulnar branch and the arterial tree distal from the radial artery are each accounted for by a lumped model.

Tube Taper

Values of the radius r_0 of the artery taken from Westerhof et al. (1969), were used at the proximal and distal ends of both the brachial

and radial arteries, and the cross-sectional areas (A_p, A_2, A_3, A_d) for the corresponding values of radius were calculated (Figure 2(a)). The area A_m at the junction of the brachial and radial arteries (Figure 2(b)) was found by taking the mean of the areas A_2 and A_3 (Figure 1(a)). Finally, the data for the brachial artery contained A_p as the area of the proximal end and A_m as the area at the distal end, while the data for the radial artery contained A_m as the area of the proximal end and A_d as the area of the distal end (Figure 2(c)). For the entire model, linear taper was used.

Finite-element Simulation

The finite element method was used to obtain a solution of the model equations and to calculate pressures and flows. For the normal case, the brachial artery was divided into nine elements, and the radial artery was divided into ten elements. The ulnar branch had only one element. There was no element either between the brachial artery and the ulnar branch or between the ulnar branch and the radial artery. For the entire model, twenty elements and twenty-one nodes were used. Wherever the stenosis was introduced in the artery, the length of the stenosis was included in the total length of the arterial section, and subsequently the length of the elements were proportionally changed. In doing so, the number of the

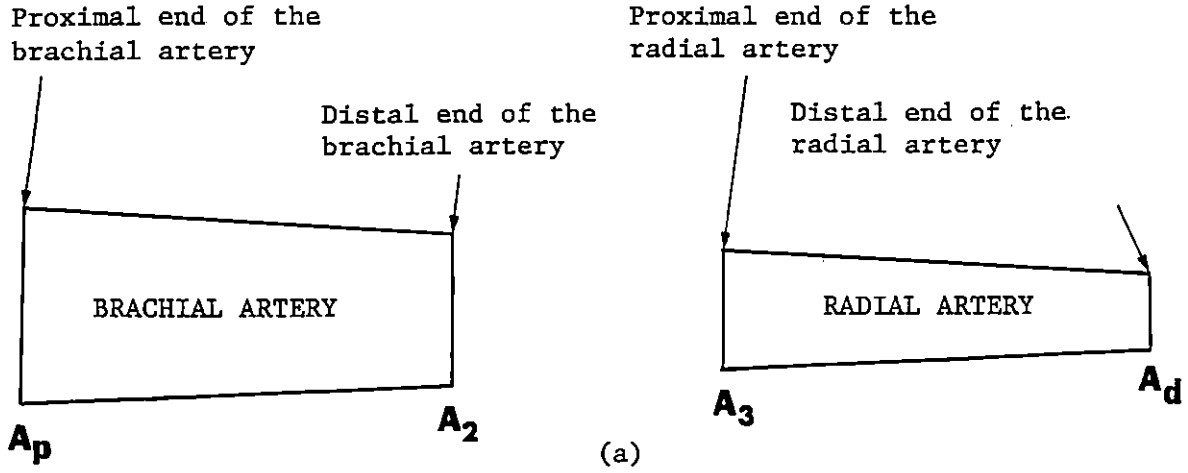

(a)

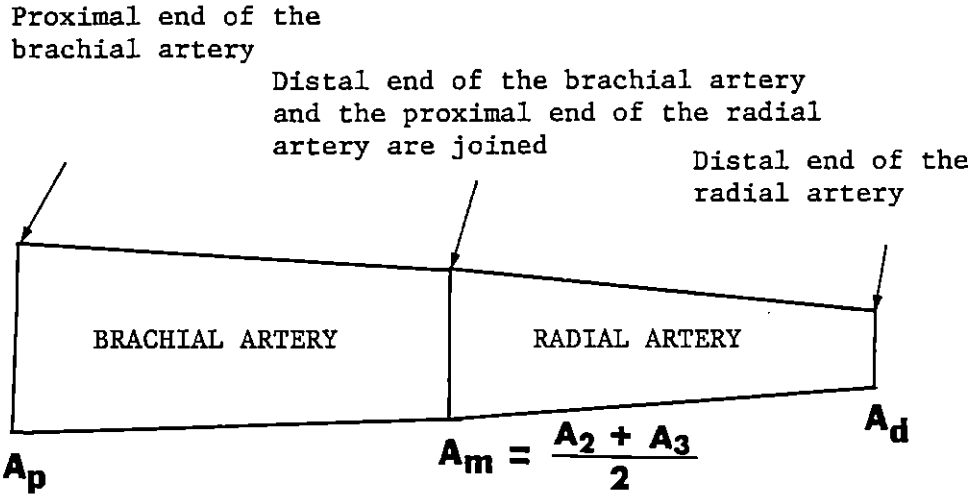

(b)

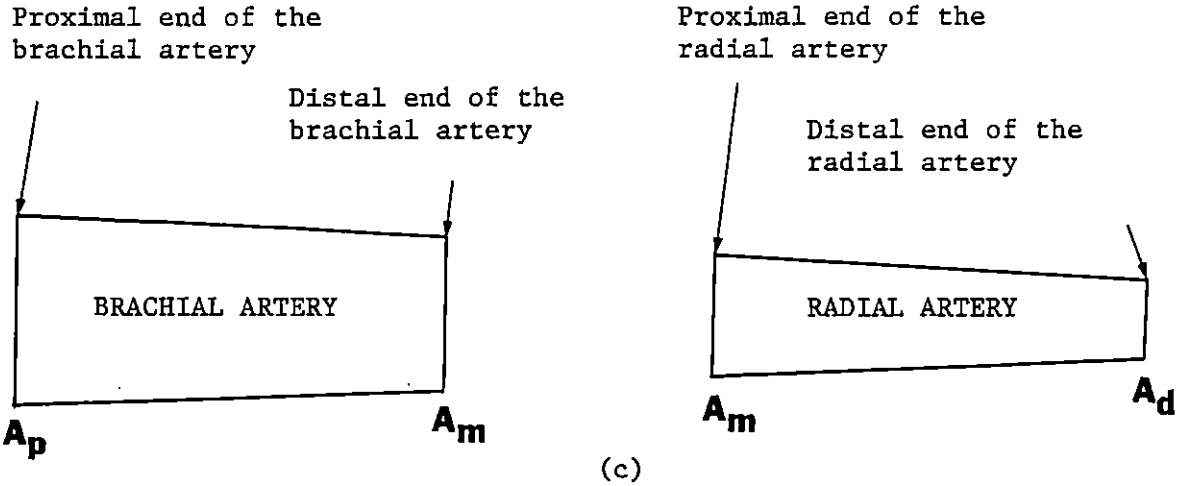

(c)

FIGURE 2. Determination of the area A_m in the present model

elements and nodes were reduced, but the total length of the arterial section was maintained constant. The detailed analysis for simulation of the model equations by the finite element method is discussed in a study by Young et al. (1981).

PHYSIOLOGICAL MODEL

The principles and assumptions of Raines et al. (1974) and Porenta (1982) (models of the human femoral artery) were considered in the development of the model of the human arm. Only the major arteries such as brachial, radial and ulnar were modeled, while the small arteries emanating from the brachial and radial arteries were neglected. Although both radial and ulnar arteries are approximately equal in diameter, and carry almost an equal amount of blood flow, the radial artery was taken as a continuation of the brachial artery, and the ulnar artery was lumped. The reason for doing this is that the radial artery is clinically more important than the ulnar artery, since pulses are measured on the radial artery, and pressure is frequently measured on the radial artery. The idea of lumping the ulnar artery is not as sound as considering bifurcation of the radial and ulnar branches and studying flow situations in both the branches equally. However, lumping of the ulnar artery makes the model relatively simple. Also, the details of the pulse propagation are sought only along the brachial and radial arteries. Figure 3 represents the schematic of the model geometry.

Arterial Dimensions and Flow Distributions

Values of lengths and radii of the brachial and radial arteries were taken from Westerhof et al. (1969) to calculate cross-sectional

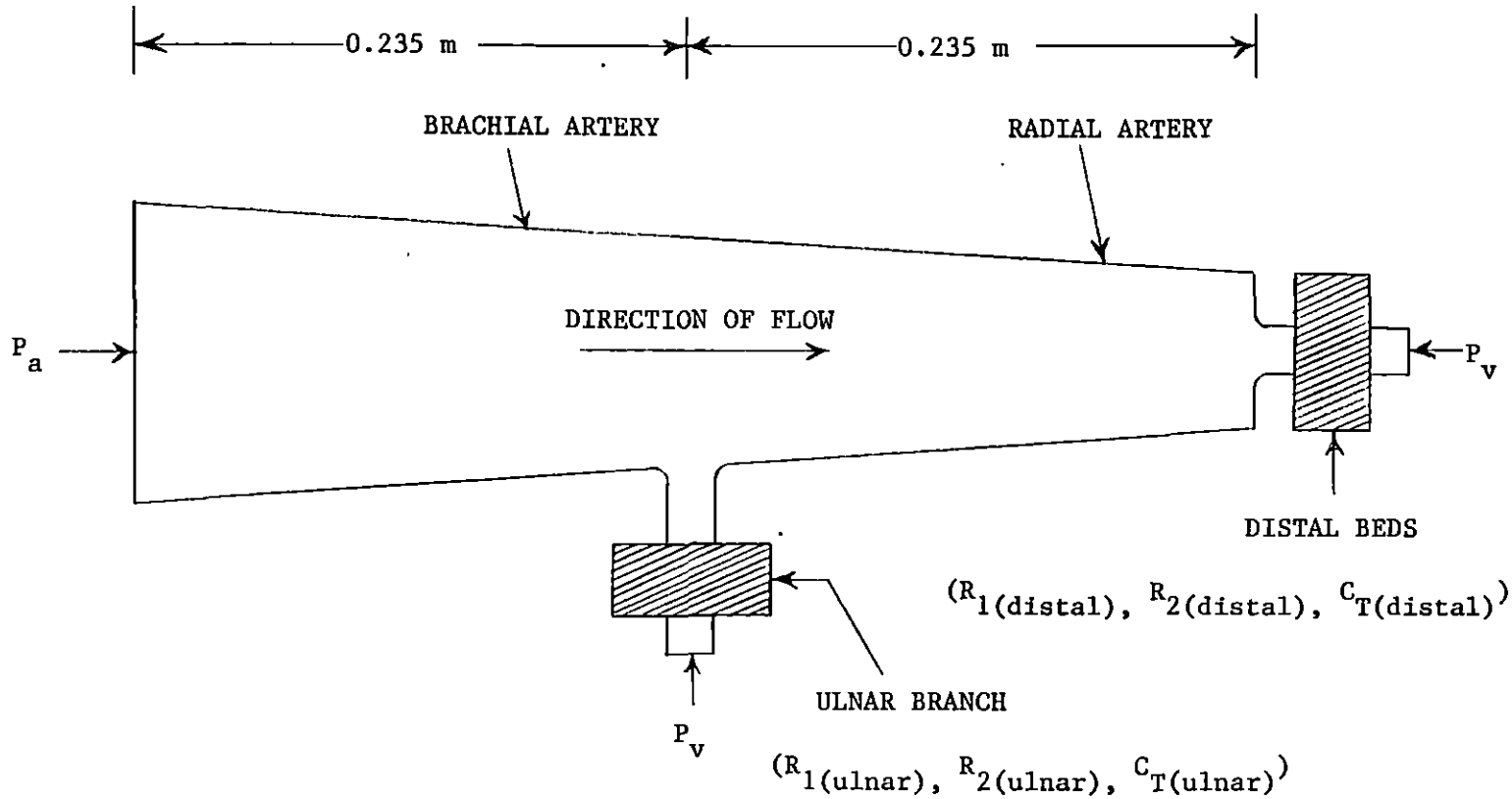

FIGURE 3. A schematic of the arteries in the human arm (P_a and P_v are the arterial and venous pressures, respectively, and (R_1, R_2, C_T) is a parameter triplet characterizing the corresponding peripheral bed.)

areas. The flow distribution was handled by following the assumptions made by Raines et al. (1974) for the femoral artery. Since the diameters of the radial and ulnar arteries are almost equal and almost half the diameter of the brachial artery, it was assumed that the flow in the brachial artery divides equally in the ulnar and radial arteries. Hence, a good approximation is to assume that the ulnar peripheral resistance $R_{T(ulnar)}$ and the distal peripheral resistance $R_{T(distal)}$ are equal, i.e.,

$$R_{T(ulnar)} = R_{T(distal)} \tag{6}$$

The mean blood flow through the brachial artery has been taken as 98 ml/min (Simon et al., 1983) and the mean pressure in the brachial artery has been considered as 95 mm Hg (Kroeker and Wood, 1955, 1956). Thus, the total peripheral resistance R of the arm is considered to be

$$R = \frac{95 \text{ mm Hg}}{98 \text{ ml/min}} = 58.163 \text{ mm Hg-sec/ml}$$

$$= 0.773 \times 10^{10} \text{ N-s/m}^5 \tag{7}$$

Also, considering the flow distribution in the arteries, one can write the following equation:

$$\frac{1}{R} = \frac{1}{R_{T(ulnar)}} + \frac{1}{R_{T(distal)}} \tag{8}$$

Using (6), (7) and (8), one finds:

$$R_{T(ulnar)} = R_{T(distal)} = 2R = 0.1546 \times 10^{11} \text{ Ns/m}^5 \tag{9}$$

As discussed by Raines et al. (1974), the peripheral

resistance R_T at each branch and termination must be divided into two resistances R_1 and R_2. The measurements of McDonald and Attinger as discussed by Raines et al. (1974) indicated that the optimum value of $R_1/R_T = 0.2$ is the value which minimizes the modulus of the reflection coefficient K at the value $|K| = 0.2$. This was the case for the femoral artery. In a similar manner, it was necessary to find a suitable ratio for the present model. In order to do this, it was first necessary to find the value of the compliance of the artery and hence to find the linear compliance term C_0, the nonlinear compliance term C_1 and the terminal lumped compliance C_T.

First, one needs to find a_0, and it can be estimated from the Moens-Korteweg equation,

$$a_0 = (Eh_0/\rho d_0)^{1/2} \tag{10}$$

From Westerhof et al. (1969) and Avolio (1980), values of Young's modulus E, arterial wall thickness h_0 and radius r_0 were taken, and converted into required units for the final form (the average values of h_0 and r_0 are used here). The value of the density ρ of the blood used here is 1050 kg/m^3, which was also used by Porenta (1982). The values obtained were as follows:

$E = 8\times10^5$ N/m^2, $\quad h_0 = 0.0525\times10^{-2}$ m

$\rho = 0.1050\times10^4$ kg/m^3, $\quad r_0 = 0.2585\times10^{-2}$ m

$d_0 = 2r_0 = 0.517\times10^{-2}$ m

Substituting the above values in equation (10), the calculated value

of a_0 was equal to 8.8 m/s which was very close to the value 8.7 m/s listed by McDonald (1974). Thus, the coefficients of the polynomial in the equation (3) can be calculated as follows:

$$C_0^a = \frac{1}{0.1050 \times 10^4 \times (8.8)^2} = 1.23 \times 10^{-5} \ m^2/N$$

$$C_1^a = (C_0^a)^2 = (1.23 \times 10^{-5})^2 = 1.51 \times 10^{-10} \ m^4/N^2$$

So that one has the linear and nonlinear compliance terms as

$$C_0 = C_0^a - 2C_1^a p_0$$

$$= [1.23 \times 10^{-5} - 2(1.51 \times 10^{-10})\ (95 \times 132.9)]$$

$$= 0.8487 \times 10^{-5} \ m^2/sN$$

$$C_1 = 2C_1^a$$

$$= 2(1.51 \times 10^{-10})$$

$$= 0.3020 \times 10^{-9} \ m^4/sN^2$$

A method outlined in Raines et al. (1974) was followed to determine the tube compliance (the arterial volumetric compliance) C_{tube} of the artery. The value of C_{tube} is used to find the value of the lumped compliance C_{lumped} for each branch of the arterial model. The compliances are related as

$$C_{lumped} = C_{total} - C_{tube}$$

where C_{total} is the total arterial volumetric compliance of the arterial model. The value of C_{total} for the brachial artery is taken from Simon et al. (1983), and is equal to 0.123×10^{-10} m^5/N. In order to find the value of C_{lumped}, an integration was performed over the

length of the artery, using the following assumptions. (1) The volumetric compliance is measured at constant pressure. In other words, one value of the volume is measured at one value of the pressure, and the second value of the volume is measured at the second value of the pressure, etc. (2) The nonlinearity term in the equation of state (equation (3)) is neglected here for two reasons: (i) To reduce the complexity of the calculations and (ii) It is very small compared to the other terms.

Thus, equation (3) can be reduced to the form,

$$A = A_0 \, [1 + C_0^a \, (p-p_0)]$$

Integrating over the length 1 of the artery, one has

$$\int_0^1 A \, dx = \int_0^1 A_0 \, [1 + C_0^a \, (p-p_0)] dx$$

As the pressure is kept constant during measurement, one can take the pressure term outside of the integral, so that

$$V = [1 + C_0^a \, (p-p_0)] \int_0^1 A_0 \, dx$$

$$V = [1 + C_0^a \, (p-p_0)] V_0$$

$$V = V_0 + C_0^a \, V_0 \, (p-p_0)$$

$$\frac{dV}{dp} = 0 + C_0^a \, V_0 \, (1-0)$$

$$\frac{dV}{dp} = C_0^a \, V_0 = C_{tube}$$

where $V_0 = 6.6602 \times 10^{-6} \ m^3$ (see Appendix A)

Thus, $C_{tube} = C_0^a \, V_0 = (1.23 \times 10^{-5}) \ (6.6602 \times 10^{-6})$

$$C_{tube} = 8.1920 \times 10^{-11} \ m^5/N \qquad (11)$$

and

$$C_{lumped} = C_{total} - C_{tube}$$

$$= 1.22\times10^{-10} - 8.1920\times10^{-11}$$

$$C_{lumped} = 4.0080\times10^{-10}$$

The terminal lumped compliance for each branch is

$$C_T = \frac{C_{lumped}}{2} = 0.20040 \times 10^{-10}\ m^5/N \qquad (12)$$

To minimize the effects of reflections on waves, an optimum value of the ratio R_1/R_T was found which minimizes the value of $|K|$. The equations used by Raines were simplified, and the values of all the parameters in those equations were found for the present model. A Fortran program was written for a PDP-11/23 computer to solve these equations. Initially, the program was run by using values from the model of Raines et al. (1974), and the variation of the modulus and the phase of the reflection coefficient K at the tibial beds with the ratio R_1/R_T were found. The plots of $|K|$ versus R_1/R_T and phase angle θ versus R_1/R_T were plotted using a plotter (Figures 4 and 5). When these plots were compared with the plots given in Raines et al. (1974), they were found to be identical. The calculated values of the hemodynamic parameters of the brachial and radial arteries were introduced in the same program (Appendix B), and the results of the plots were observed (Figures 6 and 7). It was found that the optimum value of R_1/R_T=0.1 for the minimum value of $|K|$ and hence, the ratio R_1/R_T=0.1 was considered for the arm model.

The detailed analysis for finding this ratio is as follows: Substituting $R_1 = R_1 \frac{R_T}{R_1}$ and $R_2 = R_T\left(1 - \frac{R_1}{R_T}\right)$ into equation (5) one gets,

$$Z_T = R_T(R_1/R_T) + \frac{R_T\,(1 - R_1/R_T)}{1 + (1 - R_1/R_T)\,R_T^2\,C_T^2\omega^2} - \frac{j(1 - R_1/R_T)^2\,R_T^2\,C_T\,\omega}{1 + (1-R_1/R_T)^2\,R_T^2\,C_T^2\,\omega^2} \qquad (13)$$

FIGURE 4. Magnitude of the reflection coefficient at the distal bed as a function of R_1/R_T for Raines et al.'s (1974) model

FIGURE 5. Phase of the reflection coefficient at the distal bed as a function of R_1/R_T for Raines et al.'s (1974) model

FIGURE 6. Magnitude of the reflection coefficient at the distal bed as a function of R_1/R_T for the present model of the brachial and radial arteries

FIGURE 7. Phase of the reflection coefficient at the distal bed as a function of R_1/R_T for the present model of the brachial and radial arteries

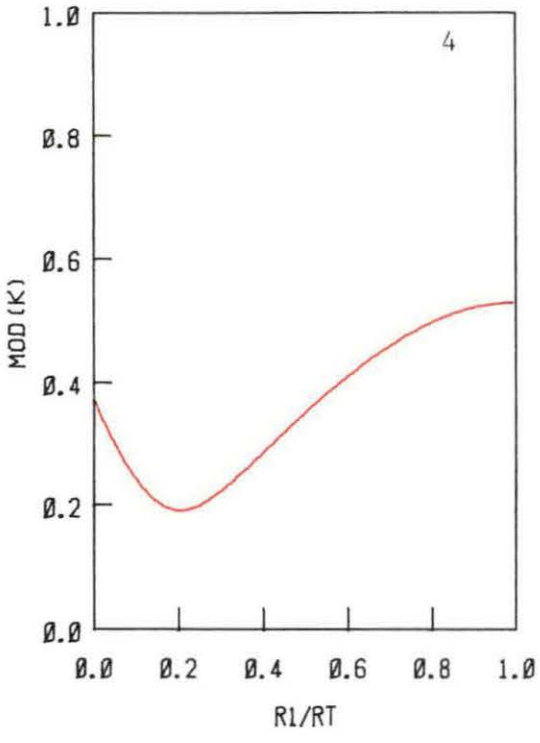
4
1.0
0.8
0.6
0.4
0.2
0.0
MOD(K)
0.0
0.2
0.4
0.6
0.8
1.0
R1/RT

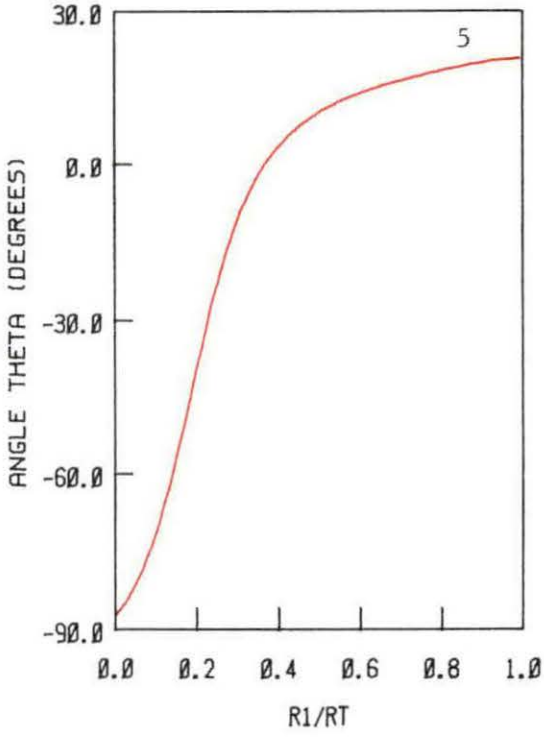
5
30.0
0.0
-30.0
-60.0
-90.0
ANGLE THETA (DEGREES)
0.0
0.2
0.4
0.6
0.8
1.0
R1/RT

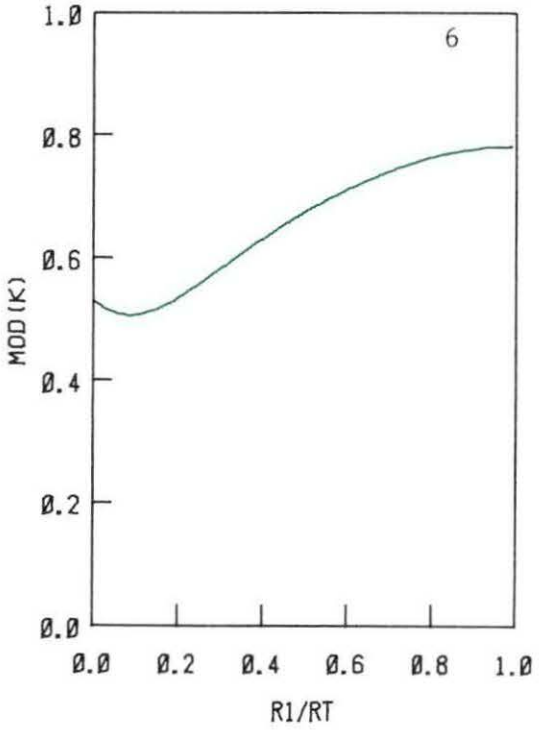
6
1.0
0.8
0.6
0.4
0.2
0.0
MOD(K)
0.0
0.2
0.4
0.6
0.8
1.0
R1/RT

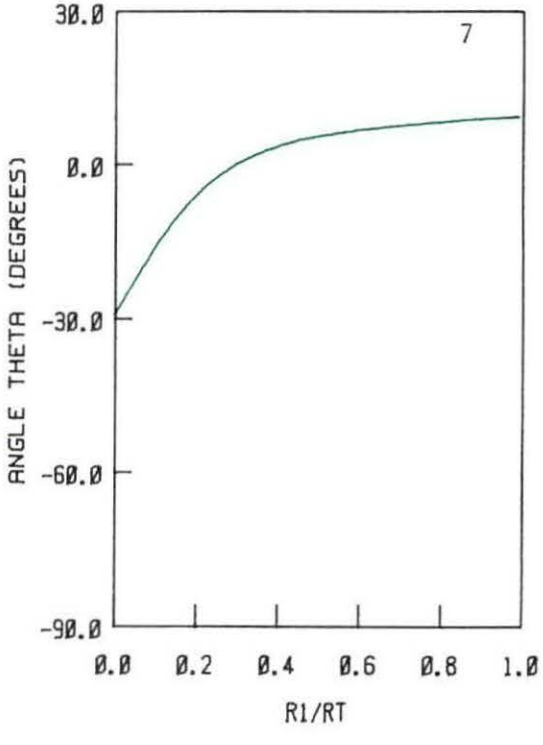
7
30.0
0.0
-30.0
-60.0
-90.0
ANGLE THETA (DEGREES)
0.0
0.2
0.4
0.6
0.8
1.0
R1/RT

Equation (8) of Raines et al. (1974) is,

$$Z_0(x) = ((4\tau/QD + j\ L_u(x)\ \omega)/j\ C_u(x)\ \omega)^{1/2}$$

where $Z_0(x)$ = local characteristic impedance of the vessel at the termination

τ = shear stress

$L_u(x)$ = inertance per unit length

$C_u(x)$ = compliance per unit length

Thus, $$(Z_0(x))^2 = (4\tau/QD + j\ L_u(x)\ \omega)/j\ C_u(x)\ \omega) \qquad (14)$$

Now, the equation for the Poiseuille flow of Raines et al. (1974) is

$$\frac{\pi\tau D}{\rho} = \frac{8\pi\ \mu Q}{\rho\ A}$$

$$\tau = \frac{8\mu Q}{AD} = \frac{8\mu Q}{(\pi/4)D^2\ D}$$

$$\frac{4\tau}{QD} = \frac{128}{\pi\ D^4} \qquad (15)$$

Substituting the above values in equation (14), one has

$$(Z_0(x))^2 = \frac{128\ \mu/\pi D^4 + j\ L_u(x)\ \omega}{j\ C_u(x)\ \omega}$$

$$= \frac{j\ C_u\ \omega}{j\ C_u\ \omega}\ \frac{(128\ \mu/\ \pi D^4 + j\ L_u(x)\ \omega)}{(j\ C_u(x)\ \omega)}$$

$$= \frac{-\ C_u\ L_u\ \omega^2 + j\ (128\mu/\pi D^4)\ C_u\ \omega}{-\ C_u\ \omega^2}$$

$$(Z_0(X))^2 = \frac{L_u}{C_u} - j\ \frac{128\ \mu}{\pi\ D^4\ C_u\ \omega}$$

$$Z_0(x) = (L_u/C_u - j\ 128\ \mu/\ \pi D^4\ C_u\ \omega)^{1/2} \qquad (16)$$

The equation for the reflection coefficients of Raines et al. (1974) is

$$K = \frac{Z_T - Z_0}{Z_T + Z_0} \tag{17}$$

where the magnitude of K is

$$K = (\text{Real}(K)^2 + \text{Imaginary}(K)^2)^{1/2} \tag{18}$$

The phase angle of K is

$$\theta = \tan^{-1} \frac{\text{Imaginary}(K)}{\text{Real}(K)} \tag{19}$$

In order to solve equations (17), (18) and (19), it was necessary to find the unknown values in the equations (14) and (16). The value of the blood viscosity μ is taken from Raines et al. (1974), and the value of the diameter D at the distal end of the radial artery is taken from Westerhof et al. (1969). Including the values obtained in the previous discussion, the required values of C_T, R_T, D and μ are as follows:

$C_T = 0.2004 \times 10^{-10}$ m^5/N

$R_T = 0.1546 \times 10^{11}$ Ns/m^5

$D = 0.0028$ m

$\mu = 0.45 \times 10^{-2}$ Ns/m^2

For the normal case, the time period is 0.77.

Thus, $\omega = 2\pi \times 1/0.77$ rad/sec

Inertance $L_u = \rho/A_0 = 0.1050 \times 10^4 / 0.06335 \times 10^{-4} = 0.16575 \times 10^9$ kg/m^5

In order to find the value of C_u (which was needed in equation (16)), the assumption (2) made earlier was followed, so that

$$C_u = A(p_0,x)\ (C_0^a)$$

$$= (0.06335\text{x}10^{-4})\ (1.23\text{x}10^{-5})\ (C_0^a \text{ is already found.})$$

$$C_u = 7.7921\text{x}10^{-4}\ m^4/N \qquad (20)$$

While writing the program, the complex quantities were handled by treating the real and imaginary parts separately, and then combining them together to find K.

Thus, by using the obtained ratio $R_1/R_T = 0.1$, we get

$$R_{1(ulnar)} = 0.1\ (R_{T(ulnar)}) = 0.1\ (0.1546\text{x}10^{11})$$

$$= 0.1546\text{x}10^{10}\ N\text{-}s/m^5 \qquad (21)$$

$$R_{2(ulnar)} = 0.9\ (R_{T(ulnar)}) = 0.9\ (0.1546\text{x}10^{11})$$

$$= 0.1391\text{x}10^{11}\ N\text{-}s/m^5 \qquad (22)$$

Similarly,

$$R_{1(distal)} = 0.1\ (R_{T(distal)}) = 0.1546\text{x}10^{10}\ N\text{-}s/m^5 \qquad (23)$$

$$R_{2(distal)} = 0.9\ (R_{T(distal)}) = 0.1391\text{x}10^{11}\ N\text{-}s/m^5 \qquad (24)$$

The heart rate was calculated from the value of the time period for the normal pressure waveform, of the brachial artery from Mason et al. (1964):

Heart rate = (1/time period) = (1/0.77 sec) (60 sec/min) (beats)

= 78 beats/min

All values of the model parameters have been entered in the Table 1.

TABLE 1. Model parameters for the control case

Parameter description	Symbol	Value	Units
heart rate		$0.78\ 10^{2}$	beats/min
blood density	ρ	$0.105\ 10^{4}$	kg/m^3
blood viscosity	μ	$0.45\ 10^{-2}$	Ns/m^2
pulse wave velocity	a_0	$0.88\ 10^{1}$	m/s
equation of state			
linear compliance term	C_0	$0.8487\ 10^{-5}$	m^2/sN
nonlinear compliance term	C_1	$0.3020\ 10^{-9}$	m^4/sN^2
ulnar branch			
first resistance	$R_{1(ulnar)}$	$0.1546\ 10^{10}$	Ns/m^5
second resistance	$R_{2(ulnar)}$	$0.1391\ 10^{11}$	Ns/m^5
terminal compliance	$C_{T(ulnar)}$	$0.2004\ 10^{-10}$	m^5/N
distal end			
first resistance	$R_{1(distal)}$	$0.1546\ 10^{10}$	Ns/m^5
second resistance	$R_{2(distal)}$	$0.1391\ 10^{11}$	Ns/m^5
terminal compliance	$C_{T(distal)}$	$0.2004\ 10^{-10}$	m^5/N

In order to apply the proximal boundary condition, the first 7 Fourier coefficients for the sine and cosine terms have been found from the normal pressure waveform of the brachial artery taken from Mason et al. (1964). The values have been listed in Table 2, and the corresponding pressure waveform plotted using those coefficients is shown in Figure 8. The obtained pressure waveform is in good agreement with the original pressure waveform taken from Mason et al. (1964).

TABLE 2. Fourier coefficients for the proximal pressure wave for the control case (time period = 0.77 seconds)

Harmonics	Cosine coefficients (N/m^2)	Sine coefficients (N/m^2)
0	$0.1015\ 10^5$	0.0
1	$-0.9154\ 10^2$	$0.2251\ 10^4$
2	$-0.9154\ 10^3$	$0.1457\ 10^4$
3	$-0.7785\ 10^3$	$-0.5809\ 10^2$
4	$-0.4535\ 10^3$	$0.2554\ 10^2$
5	$-0.2247\ 10^3$	$-0.2067\ 10^3$
6	$-0.4539\ 10^2$	$-0.1373\ 10^3$

Similarly, the Fourier coefficients for the cases of the hypertension, AS, AI and AS/AI have also been found and entered in Tables 3, 4, 5 and 6 respectively, while the corresponding pressure waveforms using these coefficients are shown in Figures 9, 10, 11 and 12

FIGURE 8. The pressure waveform obtained using the Fourier coefficients in Table 2 (for the control case)

FIGURE 9. The pressure waveform obtained using the Fourier coefficients in Table 3 (for the case of hypertension)

FIGURE 10. The pressure waveform obtained using the Fourier coefficients in Table 4 (for the case of AS (valvular aortic stenosis))

FIGURE 11. The pressure waveform obtained using the Fourier coefficients in Table 5 (for the case of AI (pure aortic regurgitation))

FIGURE 12. The pressure waveform obtained using the Fourier coefficients in Table 6 (for the case of AS/AI (combined valvular aortic stenosis and regurgitation))

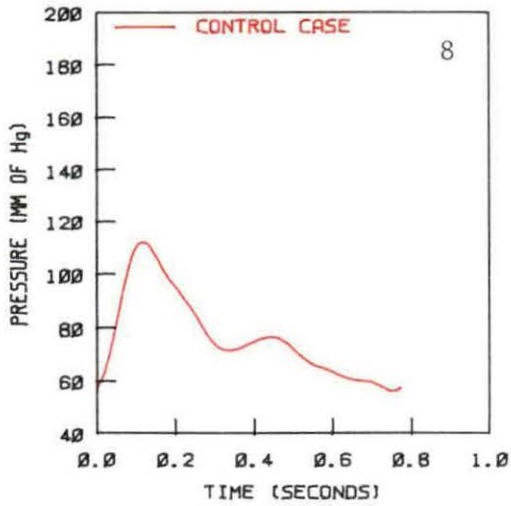
CONTROL CASE
8
PRESSURE (MM OF Hg)
200
180
160
140
120
100
80
60
40
0.0
0.2
0.4
0.6
0.8
1.0
TIME (SECONDS)

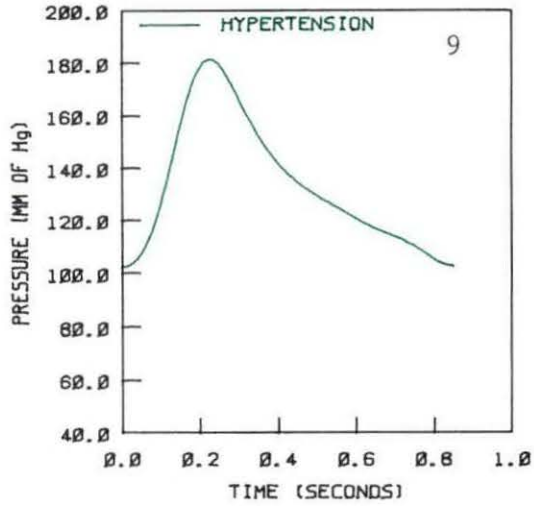
HYPERTENSION
9
PRESSURE (MM OF Hg)
200.0
180.0
160.0
140.0
120.0
100.0
80.0
60.0
40.0
0.0
0.2
0.4
0.6
0.8
1.0
TIME (SECONDS)

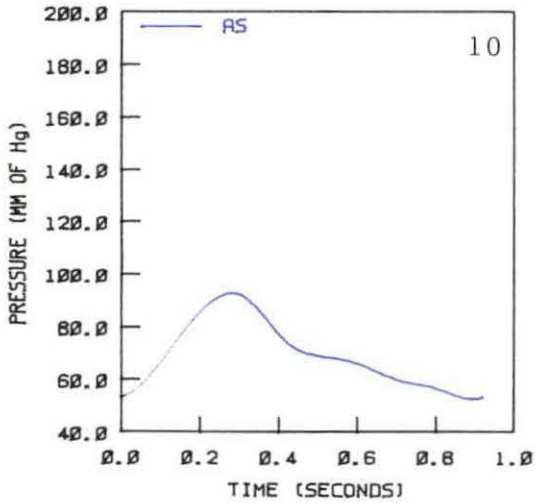
AS
10
PRESSURE (MM OF Hg)
200.0
180.0
160.0
140.0
120.0
100.0
80.0
60.0
40.0
0.0
0.2
0.4
0.6
0.8
1.0
TIME (SECONDS)

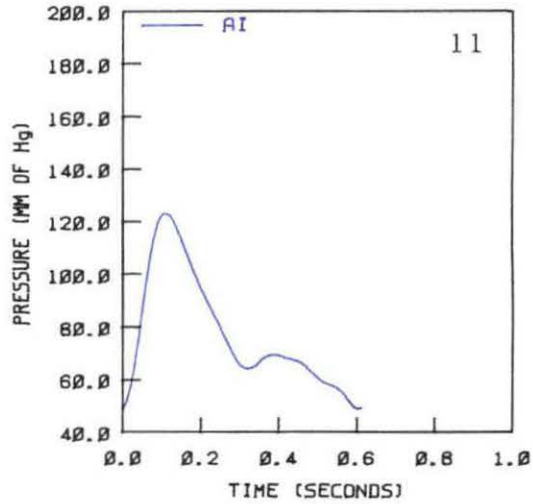
AI
11
PRESSURE (MM OF Hg)
200.0
180.0
160.0
140.0
120.0
100.0
80.0
60.0
40.0
0.0
0.2
0.4
0.6
0.8
1.0
TIME (SECONDS)

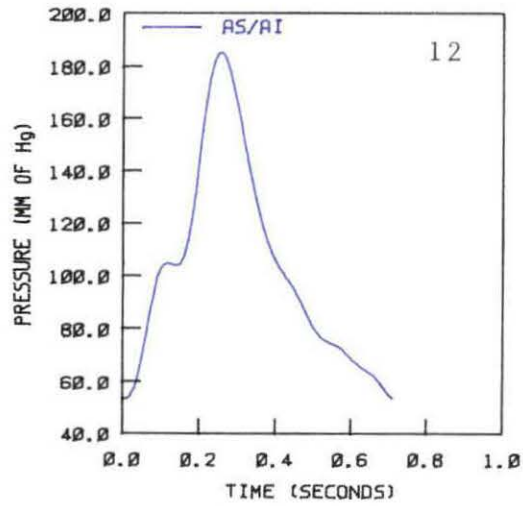
AS/AI
12
PRESSURE (MM OF Hg)
200.0
180.0
160.0
140.0
120.0
100.0
80.0
60.0
40.0
0.0
0.2
0.4
0.6
0.8
1.0
TIME (SECONDS)

respectively. The obtained pressure waveforms are in good agreement with the original waveforms taken from Simon et al. (1983) and Mason et al. (1964).

TABLE 3. Fourier coefficients for the proximal pressure wave for the case of hypertension (time period = 0.85 seconds)

Harmonics	Cosine coefficients (N/m^2)	Sine coefficients (N/m^2)
0	$0.1768\ 10^5$	0.0
1	$-0.2282\ 10^4$	$0.3372\ 10^4$
2	$-0.1922\ 10^4$	$-0.4972\ 10^3$
3	$-0.1014\ 10^3$	$-0.7780\ 10^3$
4	$0.1819\ 10^3$	$-0.9453\ 10^2$
5	$0.2950\ 10^2$	$0.6171\ 10^2$
6	$-0.1585\ 10^1$	$0.2294\ 10^2$

TABLE 4. Fourier coefficients for the proximal pressure wave for the case of AS (time period = 0.92 seconds)

Harmonics	Cosine coefficients (N/m^2)	Sine coefficients (N/m^2)
0	$0.9163\ 10^4$	0.0
1	$-0.1220\ 10^4$	$0.1778\ 10^4$
2	$-0.8915\ 10^3$	$-0.1824\ 10^3$
3	$0.1014\ 10^3$	$-0.2037\ 10^3$
4	$-0.9870\ 10^2$	$0.7092\ 10^2$
5	$-0.2155\ 10^2$	$-0.1528\ 10^2$
6	$0.1712\ 10^2$	$0.9915\ 10^1$

TABLE 5. Fourier coefficients for the proximal pressure wave for the case of AI (time period = 0.61 seconds)

Harmonics	Cosine coefficients (N/m^2)	Sine coefficients (N/m^2)
0	$0.1021\ 10^5$	0.0
1	$-0.1791\ 10^3$	$0.3146\ 10^4$
2	$-0.2028\ 10^4$	$0.1177\ 10^4$
3	$-0.7974\ 10^3$	$-0.6695\ 10^2$
4	$-0.5460\ 10^3$	$-0.3379\ 10^3$
5	$-0.5791\ 10^2$	$-0.2063\ 10^3$
6	$-0.9066\ 10^2$	$-0.1123\ 10^3$

TABLE 6. Fourier coefficients for the proximal pressure wave for the case of AS/AI (time period = 0.71 seconds)

Harmonics	Cosine coefficients (N/m^2)	Sine coefficients (N/m^2)
0	$0.1356\ 10^5$	0.0
1	$-0.5127\ 10^4$	$0.4318\ 10^4$
2	$-0.7008\ 10^3$	$-0.2086\ 10^4$
3	$0.4663\ 10^3$	$0.8137\ 10^3$
4	$-0.1167\ 10^4$	$0.1107\ 10^3$
5	$-0.1650\ 10^3$	$-0.5673\ 10^3$
6	$0.1883\ 10^3$	$-0.2674\ 10^3$

RESULTS AND DISCUSSION

Control Case

The data for the control case are given in Table 1 and Figure 3. Figures 13 and 14 represent pressure and flow waveforms, respectively, at three different locations along the artery: at the proximal end, at the point just after the branch, and at the distal end.

An amplification of the systolic pressure and an amplification of the hump following the systolic pulse were found for the pressure pulse propagating along the artery. This hump was referred to as the reflected wave by Raines et al. (1974). A decrease in amplitude of the peak flow and an occurrence of a hump at the distal end were found for the flow waveform. The mean flow reduces as a result of branching. A phase of back flow was observed along the entire arterial length. This kind of behavior for pressure and flow waves was also observed in the femoral artery by Raines et al. (1974) and Porenta (1982). These findings are also in agreement with Clark et al.'s (1974) results in brachial and radial arteries.

Figure 15 shows the inverse damping factors (IDF) of the pulsatility index (PI) for the normal case. As discussed by Porenta (1982), the pulsatility index is commonly defined as the ratio of peak to peak flow excursion to the mean flow, and IDF is defined as the ratio of a distal index measurement to a proximal index measurement. Here, the distal index measurement is the PI at the distal end, while the proximal index measurement is the PI at the proximal end. As shown in

FIGURE 13. Pressure waves along the artery for the control case

FIGURE 14. Flow waves along the artery for the control case

FIGURE 15. Inverse Damping Factors of the Pulsatility Indices for the control case

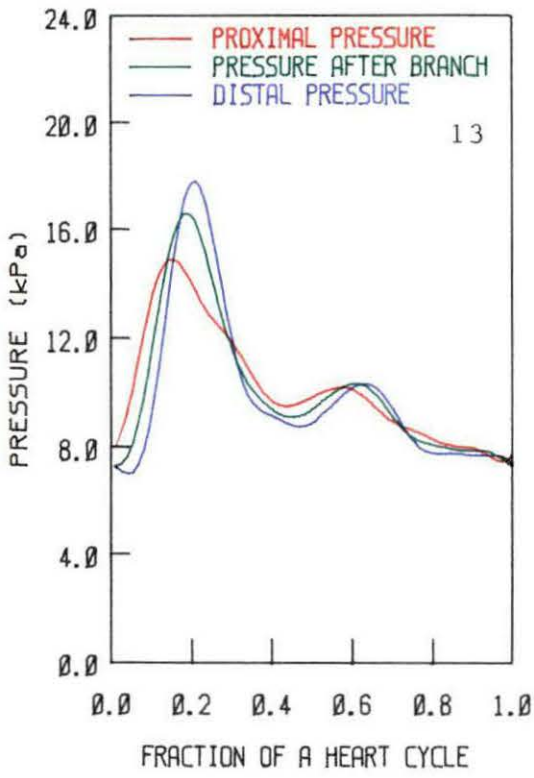
PROXIMAL PRESSURE
PRESSURE AFTER BRANCH
DISTAL PRESSURE
13
PRESSURE (kPa)
24.0
20.0
16.0
12.0
8.0
4.0
0.0
0.0
0.2
0.4
0.6
0.8
1.0
FRACTION OF A HEART CYCLE

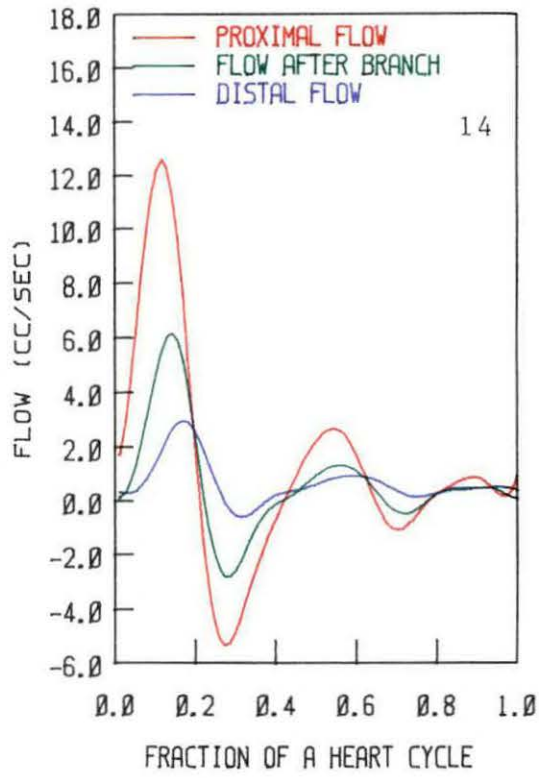
PROXIMAL FLOW
FLOW AFTER BRANCH
DISTAL FLOW
14
FLOW (CC/SEC)
18.0
16.0
14.0
12.0
10.0
8.0
6.0
4.0
2.0
0.0
-2.0
-4.0
-6.0
0.0
0.2
0.4
0.6
0.8
1.0
FRACTION OF A HEART CYCLE

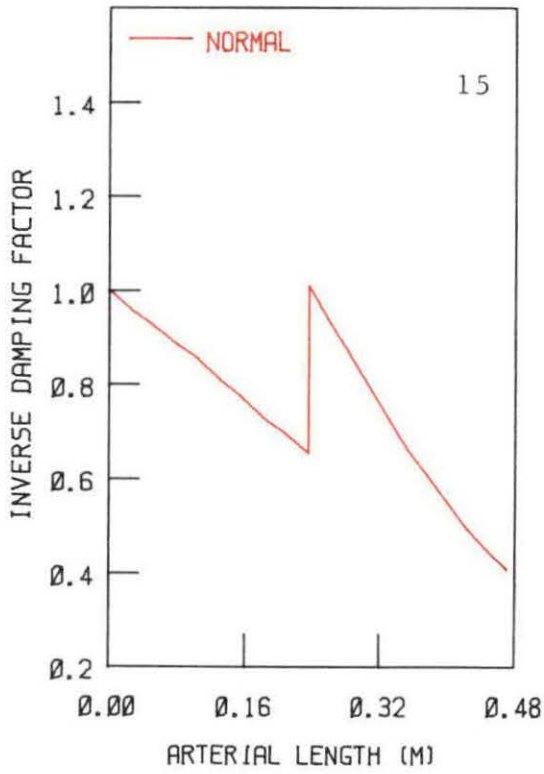
NORMAL
15
INVERSE DAMPING FACTOR
1.4
1.2
1.0
0.8
0.6
0.4
0.2
0.00
0.16
0.32
0.48
ARTERIAL LENGTH (M)

Figure 15, the proximal measurement site remains fixed at the proximal end of the brachial artery, and the distal measurement site varies along the artery. At the branch, the IDF increases suddenly as the reduction in mean flow exceeds the reduction in the difference between maximal and minimal flow rates (Porenta, 1982). Excluding the branch, one can see the tendency of decreasing IDF along the entire artery. Compared to the Porenta's (1982) results, values of IDF are much lower in the present model. In his model, the values of IDF remain above 1.0 along the entire artery except very few sites, while in the present model, the values of IDF remain below 1.0 along the artery except very few sites. The reason for this difference may be explained this way: In Porenta's (1982) model, there are two branches, and the first branch is very close to the proximal site. As a result of that, before the value of the IDF drops too much below 1.0, the flow wave reaches the first branch, and hence the value of the IDF increases rapidly and significantly above 1.0, and remains above 1.0 until the flow wave reaches the second branch. In contrast to that, in the present model, there is only one branch and that is in the middle of the artery. Thus, the values of IDF drop considerably below 1.0 when the flow wave reaches the site of the branch, and subsequently the values of IDF barely rise above 1.0 at the branch. In the remaining section, values of IDF again go down well below 1.0. Apart from the absolute values of IDF, the basic nature of the variation of the IDF along the artery seem to be the same in both Porenta's (1982) model and the present model.

Pulses of Diseased Heart Patients and a Hypertensive Patient

Flow and pressure pulses in the brachial and radial arteries indicate the general condition of the arterial system (Clark et al. 1985). Here, it is clinically important to study the pressure and flow waveforms of patients having a diseased heart, and compare these waveforms with normal waveforms. Mason et al. (1964) have recorded pressure waveforms in different patients with different diseases. Three of these pressure waveforms were considered here as a proximal boundary condition (one by one) with all other parameters remaining unchanged to recalculate the pressure distribution. Similarly, the pressure waveform of a hypertensive patient was considered as a proximal boundary condition from Simon et al. (1983).

Figures 16 and 17 represent pressure and flow waveforms of the patients having an aortic stenosis. As shown in Figure 16, one observes no amplification of systolic pulse and the hump as the pressure wave travels along the artery. As can be seen, the magnitude of the pressure waveform is not decreased much as it travels along the artery. This was not the case with normal subject (Figure 13). Thus, presence of an aortic stenosis reduces the pressure along the upper extremities. The flow at the proximal end is also reduced, but it does show further reduction after the branch and at the distal end. The flow waveform almost flattens out at the distal end. An inadequate supply of blood to the tissues may cause complications

FIGURE 16. Pressure waves along the artery for the case of AS (valvular aortic stenosis)

FIGURE 17. Flow waves along the artery for the case of AS (valvular aortic stenosis)

FIGURE 18. Pressure waves along the artery for the case of AI (pure aortic regurgitation)

FIGURE 19. Flow waves along the artery for the case of AI (pure aortic regurgitation)

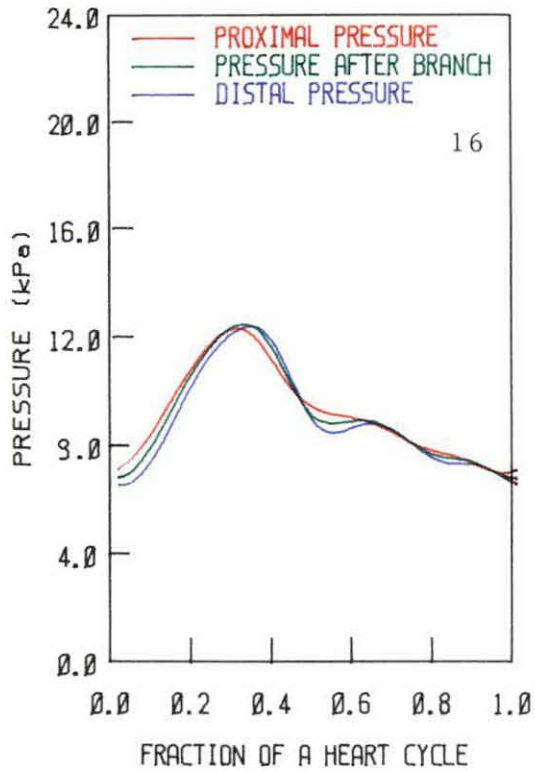
PROXIMAL PRESSURE
PRESSURE AFTER BRANCH
DISTAL PRESSURE
16
PRESSURE (kPa)
24.0
20.0
16.0
12.0
8.0
4.0
0.0
0.0
0.2
0.4
0.6
0.8
1.0
FRACTION OF A HEART CYCLE

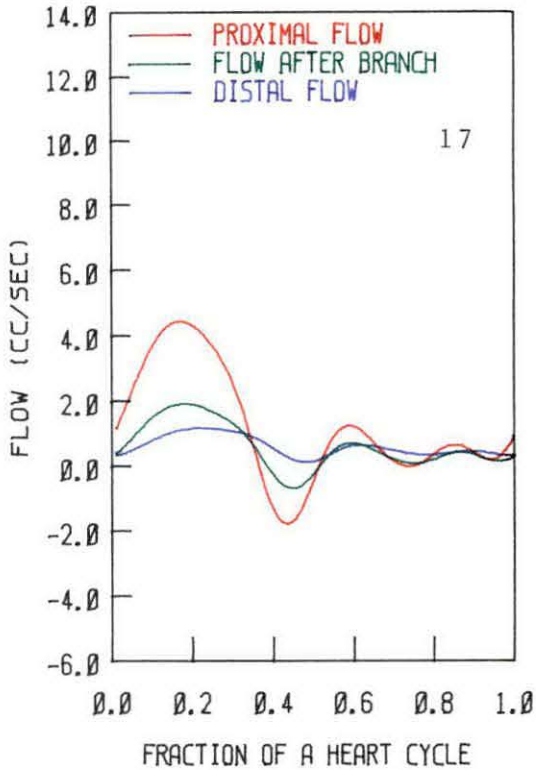
PROXIMAL FLOW
FLOW AFTER BRANCH
DISTAL FLOW
17
FLOW (CC/SEC)
14.0
12.0
10.0
8.0
6.0
4.0
2.0
0.0
-2.0
-4.0
-6.0
0.0
0.2
0.4
0.6
0.8
1.0
FRACTION OF A HEART CYCLE

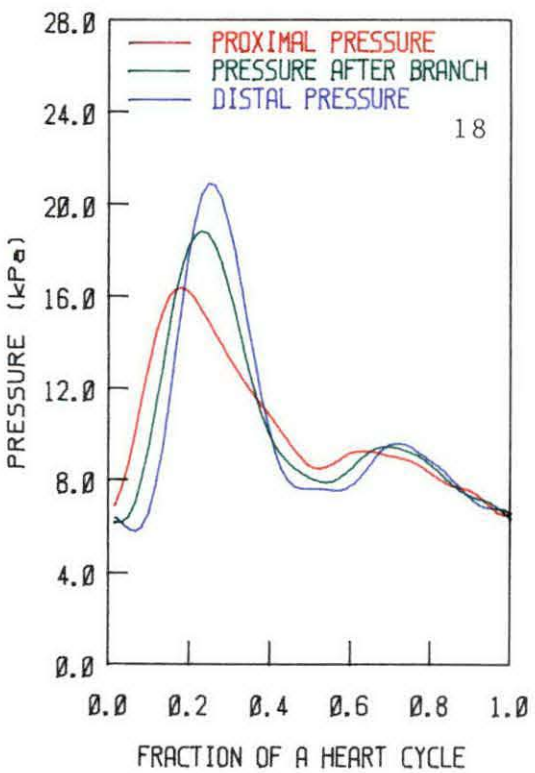
PROXIMAL PRESSURE
PRESSURE AFTER BRANCH
DISTAL PRESSURE
18
PRESSURE (kPa)
28.0
24.0
20.0
16.0
12.0
8.0
4.0
0.0
0.0
0.2
0.4
0.6
0.8
1.0
FRACTION OF A HEART CYCLE

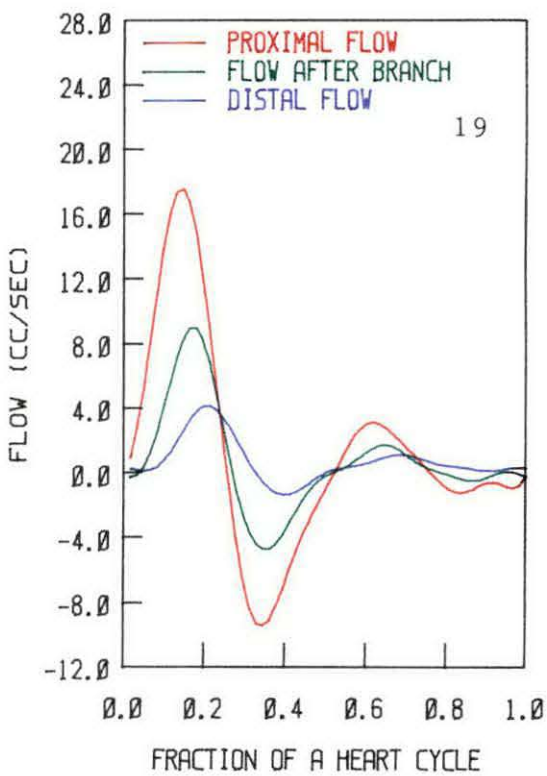
PROXIMAL FLOW
FLOW AFTER BRANCH
DISTAL FLOW
19
FLOW (CC/SEC)
28.0
24.0
20.0
16.0
12.0
8.0
4.0
0.0
-4.0
-8.0
-12.0
0.0
0.2
0.4
0.6
0.8
1.0
FRACTION OF A HEART CYCLE

in the health of a patient.

Figures 18 and 19 represent the pressure and flow waveforms, respectively, of the patient having pure aortic regurgitation. The values of mean pressure and mean flow seem slightly higher than the normal waveforms; however, the behavior of both waveforms along the arterial section in this case compared with the normal case looks very similar.

Figures 20 and 21 show the pressure and flow waveforms, respectively, of the patient having combined valvular aortic stenosis and regurgitation. The values of mean pressure and flow in this case are extremely high compared with the normal case. Also, there is an extra hump on the left hand side of the systolic pulse which may be a typical characteristic for this kind of patient. This hump is markedly high in the flow waveform. Otherwise, the behavior of the amplification of peak pressure and the magnification of the hump following the systolic pulse seems similar along the artery compared with the normal case.

Figures 22 and 23 show the pressure and flow waveforms, respectively, of the hypertensive patient. Here, the increase in amplitude of peak pressure and occurrence of a hump along the arterial section is significantly less compared with normal case. However, flow waveform does show a significant reduction in the amplitude of the peak flow as it travels along the arterial section.

Figures 24 and 25 represent the comparison of distal pressure and distal flow in the above cases. Compared to the normal waveform,

FIGURE 20. Pressure waves along the artery for the case of AS/AI (combined valvular aortic stenosis and regurgitation)

FIGURE 21. Flow waves along the artery for the case of AS/AI (combined valvular aortic stenosis and regurgitation)

FIGURE 22. Pressure waves along the artery for the case of hypertension

FIGURE 23. Flow waves along the artery for the case of hypertension

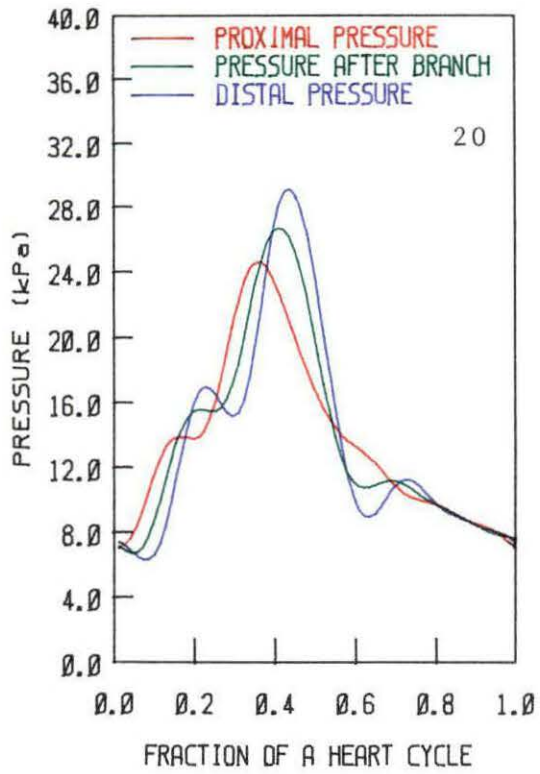
PROXIMAL PRESSURE
PRESSURE AFTER BRANCH
DISTAL PRESSURE
20
PRESSURE (kPa)
40.0
36.0
32.0
28.0
24.0
20.0
16.0
12.0
8.0
4.0
0.0
0.0
0.2
0.4
0.6
0.8
1.0
FRACTION OF A HEART CYCLE

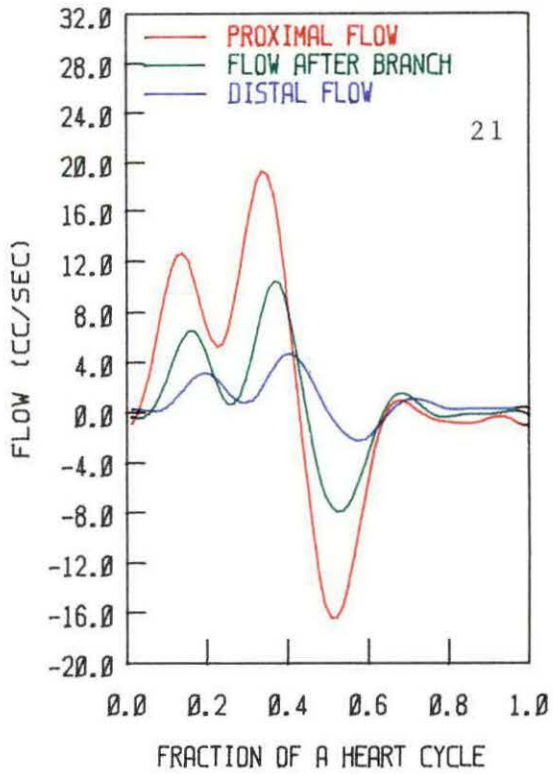
PROXIMAL FLOW
FLOW AFTER BRANCH
DISTAL FLOW
21
FLOW (CC/SEC)
32.0
28.0
24.0
20.0
16.0
12.0
8.0
4.0
0.0
-4.0
-8.0
-12.0
-16.0
-20.0
0.0
0.2
0.4
0.6
0.8
1.0
FRACTION OF A HEART CYCLE

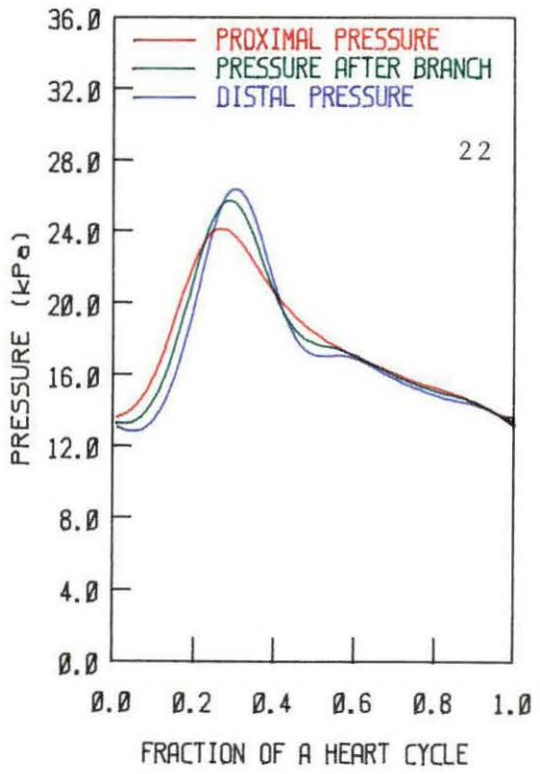
PROXIMAL PRESSURE
PRESSURE AFTER BRANCH
DISTAL PRESSURE
22
PRESSURE (kPa)
36.0
32.0
28.0
24.0
20.0
16.0
12.0
8.0
4.0
0.0
0.0
0.2
0.4
0.6
0.8
1.0
FRACTION OF A HEART CYCLE

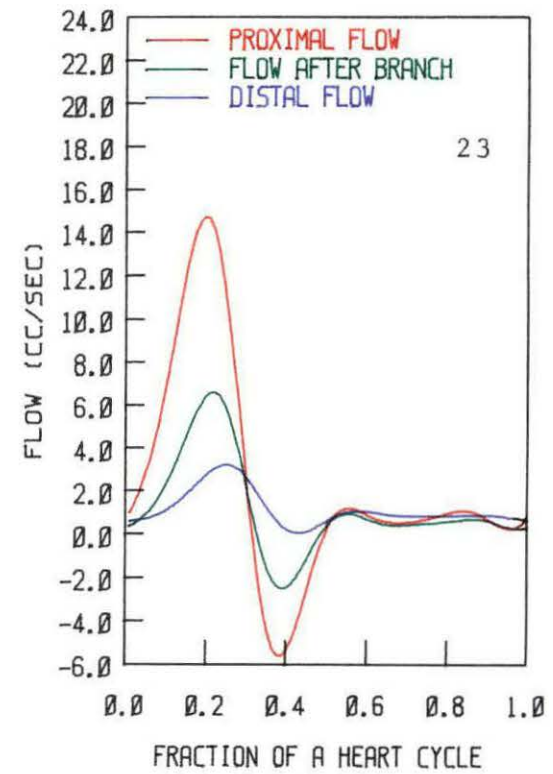
PROXIMAL FLOW
FLOW AFTER BRANCH
DISTAL FLOW
23
FLOW (CC/SEC)
24.0
22.0
20.0
18.0
16.0
14.0
12.0
10.0
8.0
6.0
4.0
2.0
0.0
-2.0
-4.0
-6.0
0.0
0.2
0.4
0.6
0.8
1.0
FRACTION OF A HEART CYCLE

FIGURE 24. Pressure waves at the distal end of the artery for the control case, cases of AS, AI, AS/AI and hypertension

FIGURE 25. Flow waves at the distal end of the artery for the control case, cases of AS, AI, AS/AI and hypertension

FIGURE 26. Inverse Damping Factors of the pulsatility indices for the control case and for the cases of AS, AI, AS/AI and hypertension

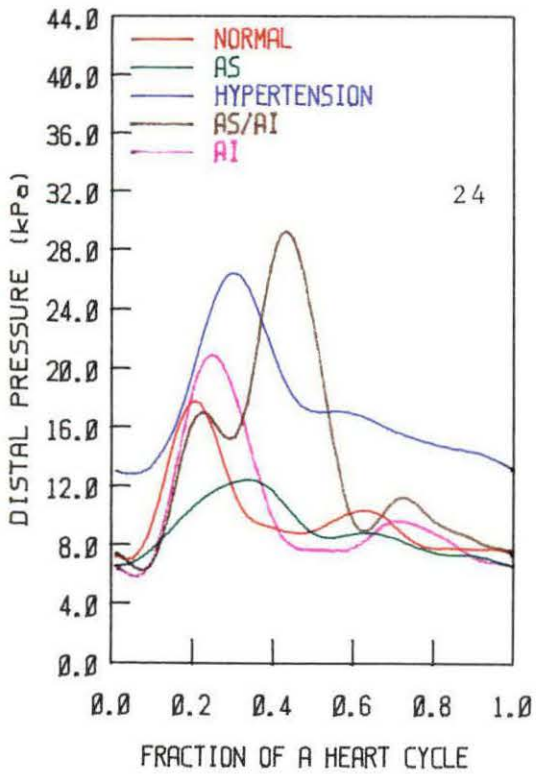
NORMAL
AS
HYPERTENSION
AS/AI
AI
24
DISTAL PRESSURE (kPa)
44.0
40.0
36.0
32.0
28.0
24.0
20.0
16.0
12.0
8.0
4.0
0.0
0.0
0.2
0.4
0.6
0.8
1.0
FRACTION OF A HEART CYCLE

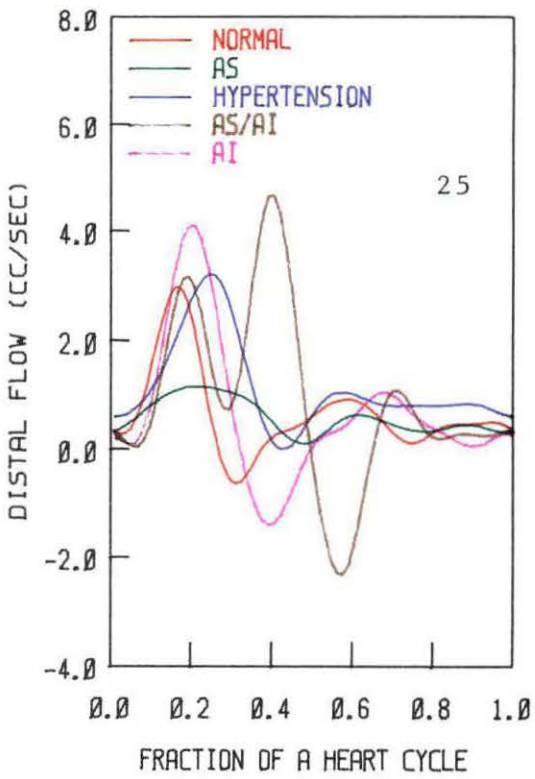
NORMAL
AS
HYPERTENSION
AS/AI
AI
25
DISTAL FLOW (CC/SEC)
8.0
6.0
4.0
2.0
0.0
-2.0
-4.0
0.0
0.2
0.4
0.6
0.8
1.0
FRACTION OF A HEART CYCLE

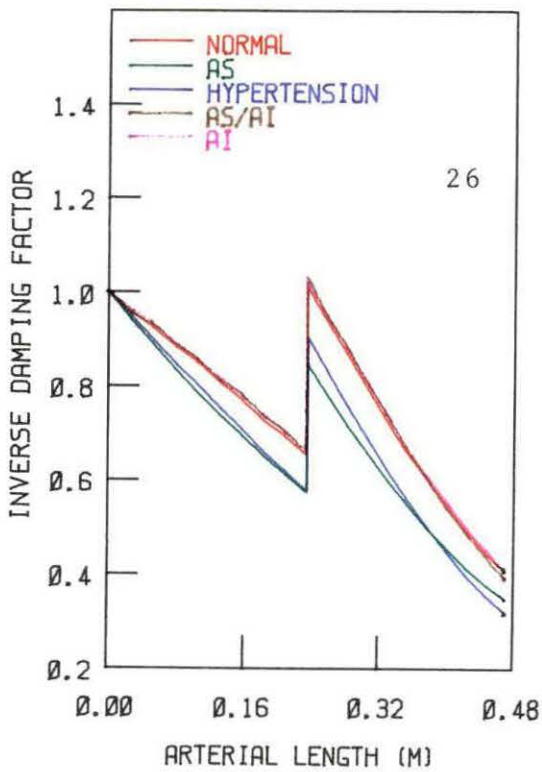
NORMAL
AS
HYPERTENSION
AS/AI
AI
26
INVERSE DAMPING FACTOR
1.4
1.2
1.0
0.8
0.6
0.4
0.2
0.00
0.16
0.32
0.48
ARTERIAL LENGTH (M)

the rest of the waveforms (at the distal end of the artery) differ in amplitude of the systolic pulse as well as in phase. This kind of overall picture certainly helps in studying the various clinical situations, and makes it easier to compare one situation with another, hence providing a diagnostic tool which may be helpful in assessing clinical problems. Figure 26 shows the IDFs of PI of above cases.

Stenosed Arteries

Even though the presence of stenoses is not commonplace in the brachial and radial arteries, stenoses were introduced in these arteries to study their effect on the pressure and flow waveforms at the distal end of the arterial section.

By keeping stenosis length constant at 0.01 m, different degrees of occlusions were placed both in brachial and radial arteries at the middle of these arteries, one by one and also in pairs. Later, a 0.1 m long stenosis was introduced in a similar manner to study the effect of long stenoses.

A single stenosis

Figures 27 and 28 show the pressure and flow waveforms, respectively, for the case of a 90% occlusion of the lumen area in the brachial artery at a distance of 0.1175 m from the proximal end. Since the stenosis is located between the proximal end and the branch-site, one can see a very low systolic pressure just after the

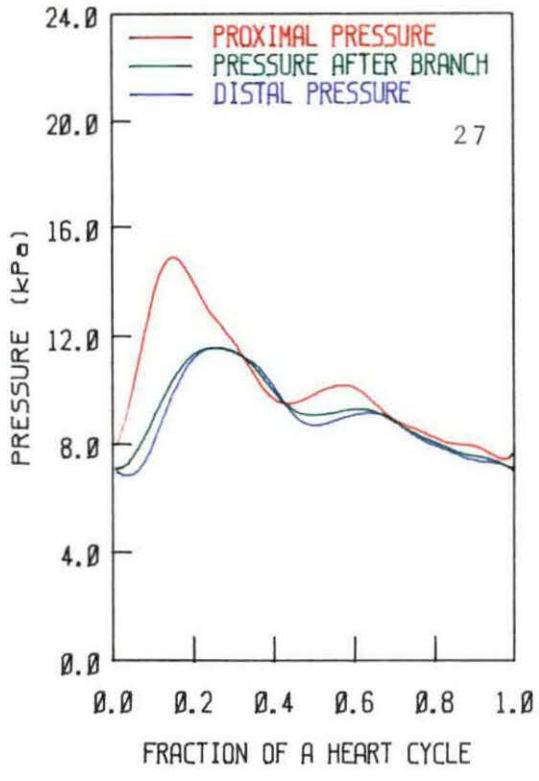
PROXIMAL PRESSURE
PRESSURE AFTER BRANCH
DISTAL PRESSURE
27
PRESSURE (kPa)
24.0
20.0
16.0
12.0
8.0
4.0
0.0
0.0
0.2
0.4
0.6
0.8
1.0
FRACTION OF A HEART CYCLE

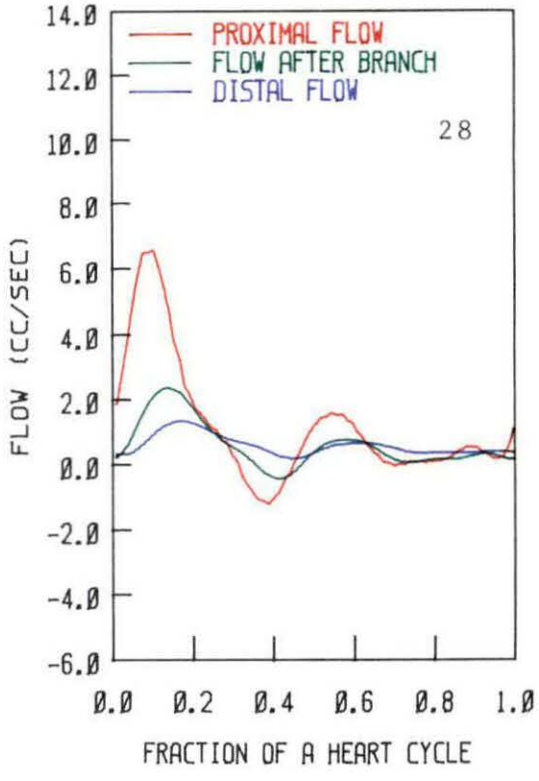
PROXIMAL FLOW
FLOW AFTER BRANCH
DISTAL FLOW
28
FLOW (CC/SEC)
14.0
12.0
10.0
8.0
6.0
4.0
2.0
0.0
-2.0
-4.0
-6.0
0.0
0.2
0.4
0.6
0.8
1.0
FRACTION OF A HEART CYCLE

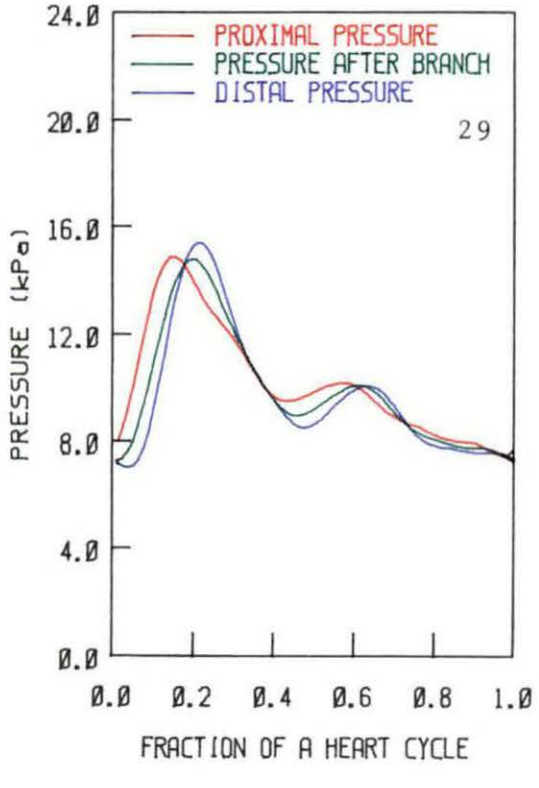
PROXIMAL PRESSURE
PRESSURE AFTER BRANCH
DISTAL PRESSURE
29
PRESSURE (kPa)
24.0
20.0
16.0
12.0
8.0
4.0
0.0
0.0
0.2
0.4
0.6
0.8
1.0
FRACTION OF A HEART CYCLE

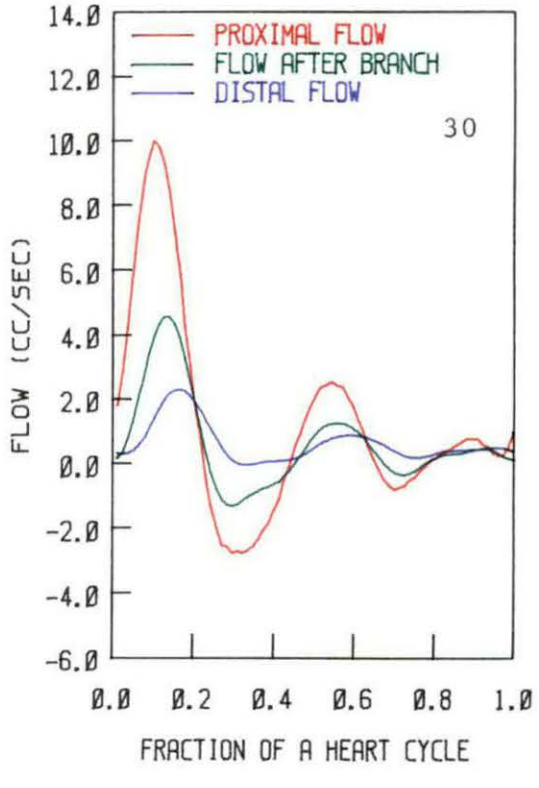
PROXIMAL FLOW
FLOW AFTER BRANCH
DISTAL FLOW
30
FLOW (CC/SEC)
14.0
12.0
10.0
8.0
6.0
4.0
2.0
0.0
-2.0
-4.0
-6.0
0.0
0.2
0.4
0.6
0.8
1.0
FRACTION OF A HEART CYCLE

branch due to the large pressure drop across the stenosis. Also, after this amount of pressure drop, pressure between the branch-site and the distal end does not drop much more. The flow waveform distal to the stenosis is also damped, and the degree of back flow is reduced at the distal end. As shown in Figure 35, the IDFs for the pulsatility indices drop very suddenly in the vicinity of the stenosis, and drop a little slower downstream of the stenosis. The absolute values of IDFs for 90% stenosis are much lower compared to that of the normal case. In short, the effect of a 90% stenosis in the brachial artery is very apparent, and easy to diagnose.

Figures 29 and 30 show the results of less severe stenosis (75%) at the same location in the brachial artery. Here, the pressure drop across the stenosis is much less, and in the radial artery this effect is overcome, and there is an increase in pressure at the distal end. Flow also does not dampen out very severely compared to the 90% stenosis case. As shown in Figure 35, IDFs of the pulsatility indices for this case do not drop very suddenly in the vicinity of the stenosis compared to the 90% stenosis case. The IDFs of the pulsatility indices for 50% stenosis are also shown in this figure, and they are almost identical to those for the normal case.

In summary, a 50% stenosed artery behaves almost like a normal artery. The 75% stenosed artery has more severe effect than the normal artery, while the 90% stenosed artery has a very severe effect.

It is interesting to investigate what happens when the same length and same degree of stenosis is placed in the middle of the

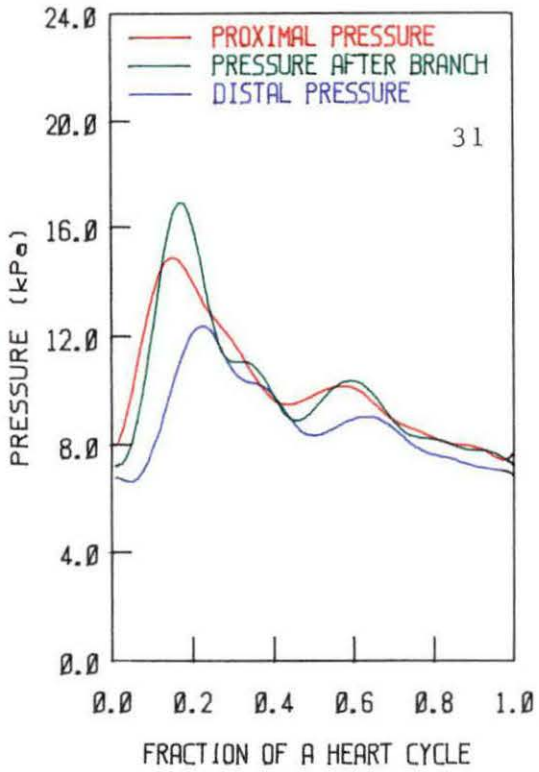
PROXIMAL PRESSURE
PRESSURE AFTER BRANCH
DISTAL PRESSURE
31
PRESSURE (kPa)
24.0
20.0
16.0
12.0
8.0
4.0
0.0
0.0
0.2
0.4
0.6
0.8
1.0
FRACTION OF A HEART CYCLE

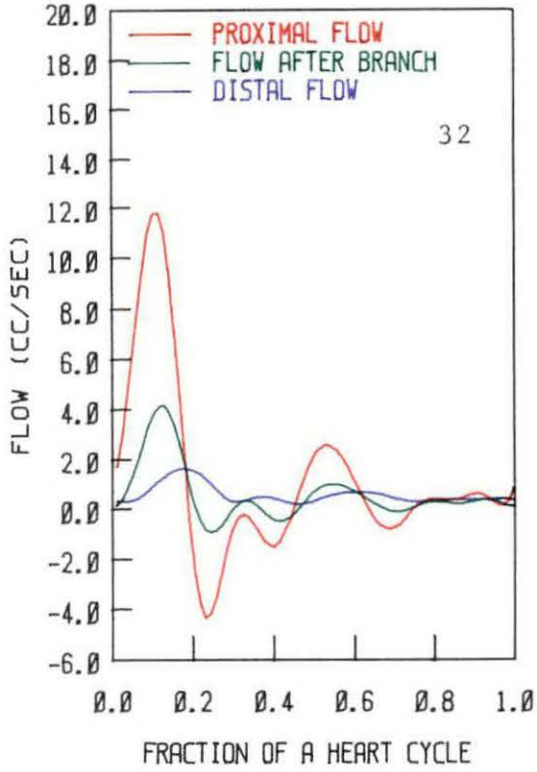
PROXIMAL FLOW
FLOW AFTER BRANCH
DISTAL FLOW
32
FLOW (CC/SEC)
20.0
18.0
16.0
14.0
12.0
10.0
8.0
6.0
4.0
2.0
0.0
-2.0
-4.0
-6.0
0.0
0.2
0.4
0.6
0.8
1.0
FRACTION OF A HEART CYCLE

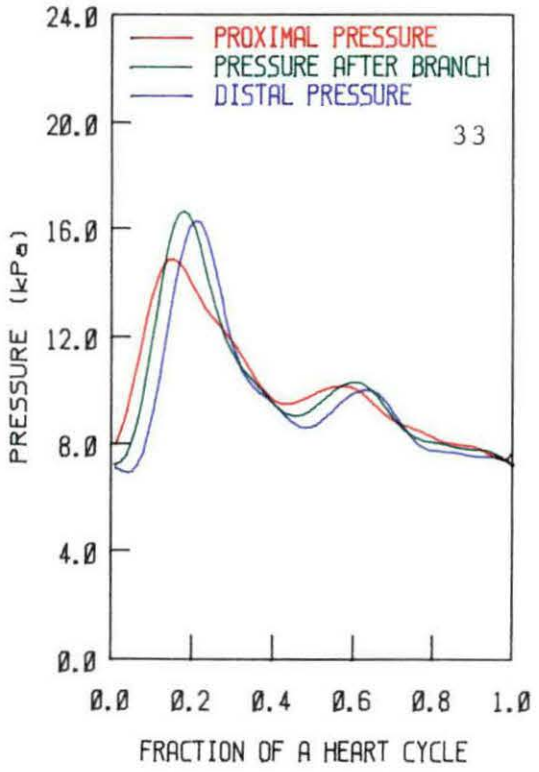
PROXIMAL PRESSURE
PRESSURE AFTER BRANCH
DISTAL PRESSURE
33
PRESSURE (kPa)
24.0
20.0
16.0
12.0
8.0
4.0
0.0
0.0
0.2
0.4
0.6
0.8
1.0
FRACTION OF A HEART CYCLE

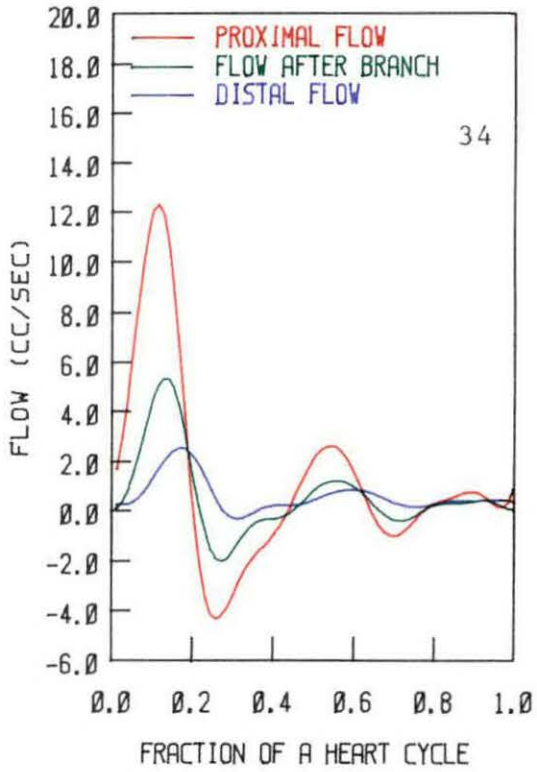
PROXIMAL FLOW
FLOW AFTER BRANCH
DISTAL FLOW
34
FLOW (CC/SEC)
20.0
18.0
16.0
14.0
12.0
10.0
8.0
6.0
4.0
2.0
0.0
-2.0
-4.0
-6.0
0.0
0.2
0.4
0.6
0.8
1.0
FRACTION OF A HEART CYCLE

FIGURE 35. Inverse Damping Factors of the Pulsatility Indices for the control case and for the cases of
(a) a 50% stenosis in the brachial artery and a 0% stenosis in the radial artery
(b) a 75% stenosis in the brachial artery and a 0% stenosis in the radial artery
(c) a 90% stenosis in the brachial artery and a 0% stenosis in the radial artery

FIGURE 36. Inverse Damping Factors of the Pulsatility Indices for the control case and for the cases of
(a) a 0% stenosis in the brachial artery and a 50% stenosis in the radial artery
(b) a 0% stenosis in the brachial artery and a 75% stenosis in the radial artery
(c) a 0% stenosis in the brachial artery and a 90% stenosis in the radial artery

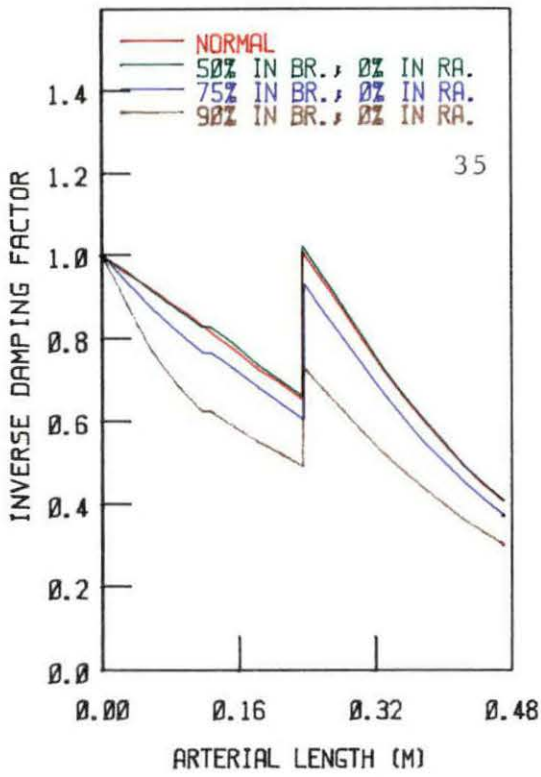
NORMAL
50% IN BR.; 0% IN RA.
75% IN BR.; 0% IN RA.
90% IN BR.; 0% IN RA.
35
INVERSE DAMPING FACTOR
1.4
1.2
1.0
0.8
0.6
0.4
0.2
0.0
0.00
0.16
0.32
0.48
ARTERIAL LENGTH (M)

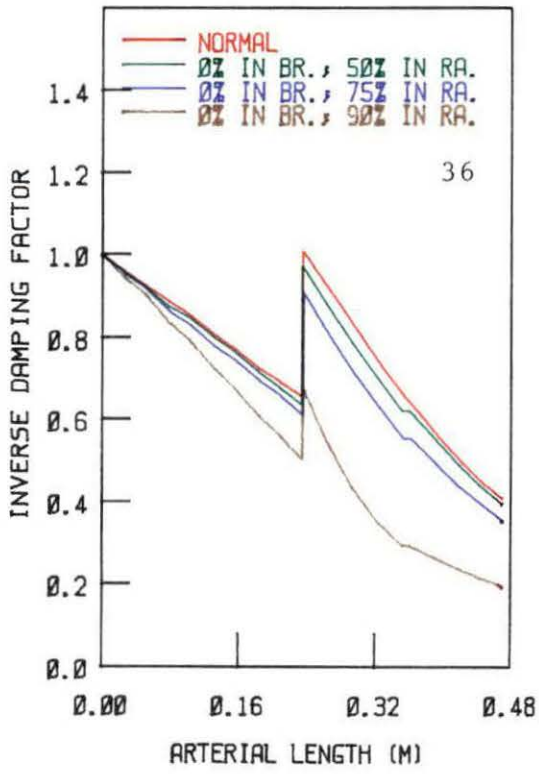
NORMAL
0% IN BR.; 50% IN RA.
0% IN BR.; 75% IN RA.
0% IN BR.; 90% IN RA.
36
INVERSE DAMPING FACTOR
1.4
1.2
1.0
0.8
0.6
0.4
0.2
0.0
0.00
0.16
0.32
0.48
ARTERIAL LENGTH (M)

radial artery instead of the brachial artery. All above combinations of stenosed brachial artery were repeated for the radial artery.

Figures 31 and 32 show the pressure and flow waveforms, respectively, when 90% stenosis is introduced in the mid-section of the radial artery (while there is no stenosis in the brachial artery). As can be seen, the amplitude of the systolic pressure in the brachial artery is a little less compared to the normal case, while the amplitude of the systolic pressure at the distal end of the radial artery is much less because of the large pressure drop across the stenosis in the radial artery. Also, the flow reduces slightly faster than the normal rate, and becomes low at the distal end. The mean values of both pressure and flow are higher than that in the case of 90% stenosis in the brachial artery (compare with Figures 27 and 28). Another interesting observation was an appearance of reflection between peak of the waveform and the hump both in the pressure and flow waveforms. Figure 36 shows the IDFs of the pulsatility indices for this case. Here, right from the proximal end of the brachial artery up to the point just before the stenosis in the radial artery, the value of IDFs drop suddenly compared to the normal case. Also, the value of IDF at the distal end is less compared to that in the case of the stenosed brachial artery.

Figures 33 and 34 show the pressure and flow waveforms, respectively, when 75% stenosis is introduced in the radial artery. The effects of stenosis is less severe compared to the cases of 90% stenosis in radial artery and 75% senosis in the brachial artery. The

FIGURE 37. Pressure waves at the distal end of the artery for the control case and for the cases of
(a) a 50% stenosis in the brachial artery and a 0% stenosis in the radial artery
(b) a 75% stenosis in the brachial artery and a 0% stenosis in the radial artery
(c) a 90% stenosis in the brachial artery and a 0% stenosis in the radial artery

FIGURE 38. Flow waves at the distal end of the artery for the control case and for the cases of
(a) a 50% stenosis in the brachial artery and a 0% stenosis in the radial artery
(b) a 75% stenosis in the brachial artery and a 0% stenosis in the radial artery
(c) a 90% stenosis in the brachial artery and a 0% stenosis in the radial artery

FIGURE 39. Pressure waves at the distal end of the artery for the control case and for the cases of
(a) a 0% stenosis in the brachial artery and a 50% stenosis in the radial artery
(b) a 0% stenosis in the brachial artery and a 75% stenosis in the radial artery
(c) a 0% stenosis in the brachial artery and a 90% stenosis in the radial artery

FIGURE 40. Flow waves at the distal end of the artery for the control case and for the cases of
(a) a 0% stenosis in the brachial artery and a 50% stenosis in the radial artery
(b) a 0% stenosis in the brachial artery and a 75% stenosis in the radial artery
(c) a 0% stenosis in the brachial artery and a 90% stenosis in the radial artery

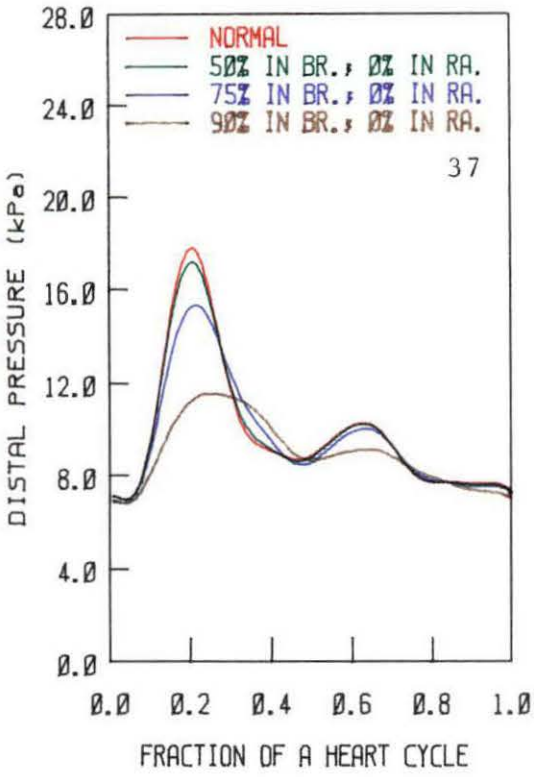
NORMAL
50% IN BR.; 0% IN RA.
75% IN BR.; 0% IN RA.
90% IN BR.; 0% IN RA.
37
DISTAL PRESSURE (kPa)
28.0
24.0
20.0
16.0
12.0
8.0
4.0
0.0
0.0
0.2
0.4
0.6
0.8
1.0
FRACTION OF A HEART CYCLE

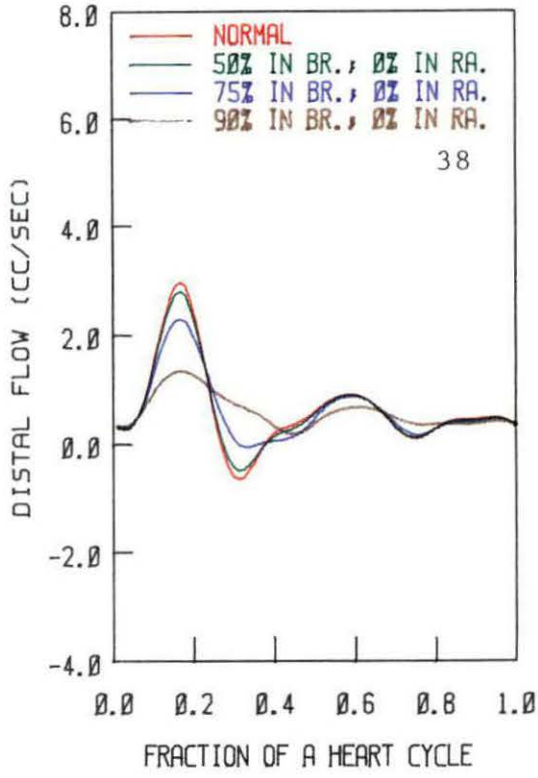
NORMAL
50% IN BR.; 0% IN RA.
75% IN BR.; 0% IN RA.
90% IN BR.; 0% IN RA.
38
DISTAL FLOW (CC/SEC)
8.0
6.0
4.0
2.0
0.0
-2.0
-4.0
0.0
0.2
0.4
0.6
0.8
1.0
FRACTION OF A HEART CYCLE

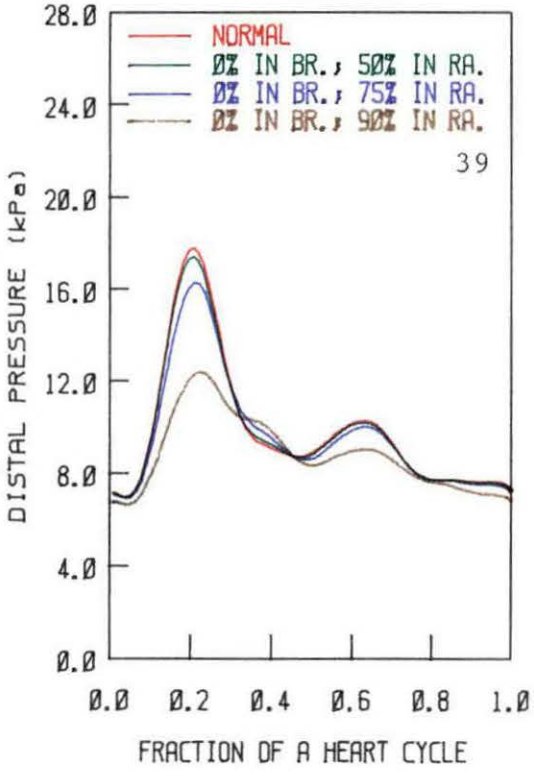
NORMAL
0% IN BR.; 50% IN RA.
0% IN BR.; 75% IN RA.
0% IN BR.; 90% IN RA.
39
DISTAL PRESSURE (kPa)
28.0
24.0
20.0
16.0
12.0
8.0
4.0
0.0
0.0
0.2
0.4
0.6
0.8
1.0
FRACTION OF A HEART CYCLE

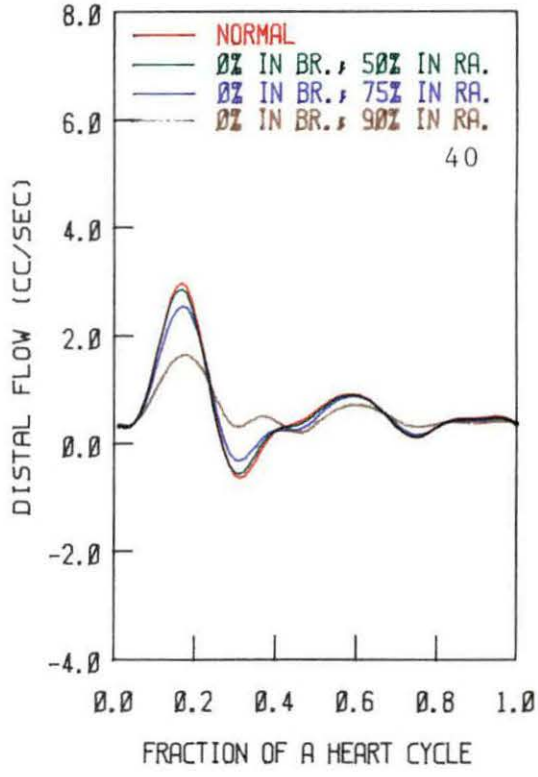
NORMAL
0% IN BR.; 50% IN RA.
0% IN BR.; 75% IN RA.
0% IN BR.; 90% IN RA.
40
DISTAL FLOW (CC/SEC)
8.0
6.0
4.0
2.0
0.0
-2.0
-4.0
0.0
0.2
0.4
0.6
0.8
1.0
FRACTION OF A HEART CYCLE

IDFs of PI for this case as shown in Figure 36 also have less severe effect compared to 90% stenosis. Figure 36 also shows the IDFs for 50% stenosis case. Values of IDFs for the stenosed radial artery are much less compared to the values of IDFs for the stenosed brachial artery (compare Figures 35 and 36).

Figures 37 and 38 represent the comparison of distal pressures and distal flows, respectively, for the cases of 50%, 75% and 90% stenosis in the brachial artery and no stenosis in the radial artery. As percent of stenosis increases, the degree of dampening of both pressure and flow waves increases. The hump in the pressure wave of 90% stenosis is dampened out severely, and there is no back flow for the case of 90% stenosis.

Figures 39 and 40 show similar comparison when the same degree of stenosis are introduced in the radial artery and no stenosis in the brachial artery. The degree of dampening of waves are less compared to the above cases of stenosed brachial artery.

Figure 41 shows the variation of IDFs of PI at the distal end with the different degree of stenosis in the brachial artery. It can be represented in a smooth curve. Figure 42 shows the similar case of the stenosed radial artery.

Dual stenoses

Another interesting set of results was obtained when different degree of stenoses were introduced in both brachial and radial arteries at the same time. Figures 43 and 44 show the distal pressure

FIGURE 41. Variation of Inverse Damping Factors of the Pulsatility Indices with the different degree of stenoses in the brachial artery

FIGURE 42. Variation of Inverse Damping Factors of the Pulsatility Indices with the different degree of stenoses in the radial artery

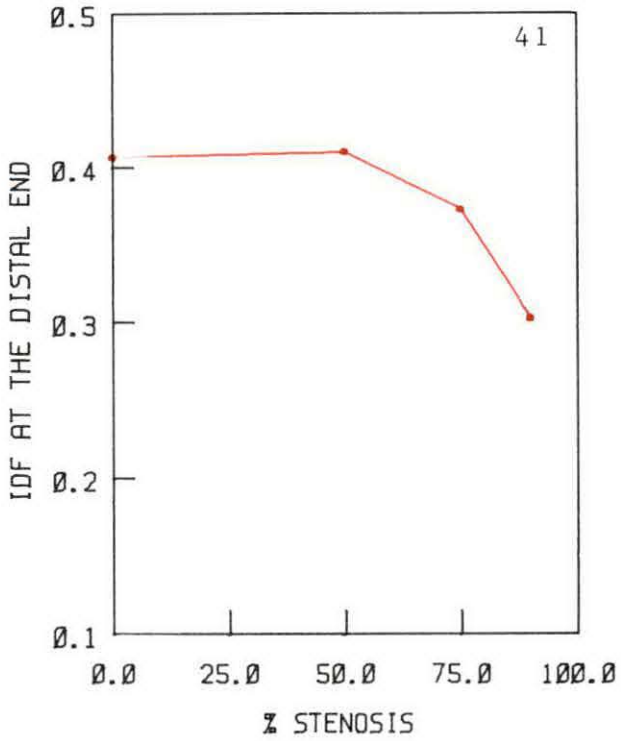
41
0.5
0.4
0.3
0.2
0.1
IDF AT THE DISTAL END
0.0
25.0
50.0
75.0
100.0
% STENOSIS

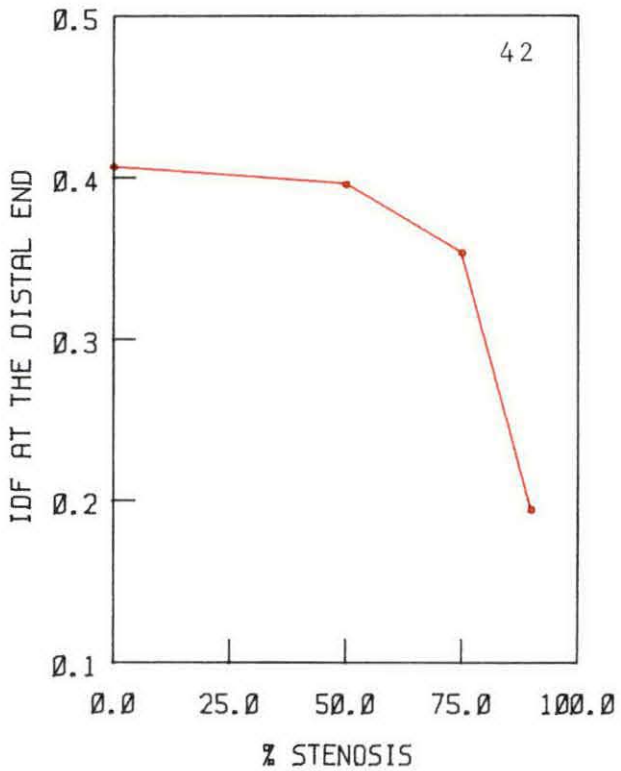
42
0.5
0.4
0.3
0.2
0.1
IDF AT THE DISTAL END
0.0
25.0
50.0
75.0
100.0
% STENOSIS

and distal flow waveforms for different combinations of stenosis in the two arteries. If we arrange these cases in order of increasing dampening effects on the waves due to the stenosis effect, it behaves as follows: normal, 75% stenosis in brachial and 75% stenosis in radial, 50% stenosis in brachial and 90% stenosis in radial, 75% stenosis in brachial and 90% stenosis in radial, 90% stenosis in brachial and 50% stenosis in radial, 90% stenosis in brachial and 75% stenosis in radial, 90% stenosis in brachial and 90% stenosis in radial. Both flow and pressure waves damp out in the same order. Effect of two stenoses are more severe compared to the individual stenoses. For example, when one compares the cases of 90% stenosis in the brachial artery only, or 90% stenosis in the radial artery only, and 90% stenosis in both brachial and radial arteries, one can distinguish the degree of dampening for the each case. Figure 45 shows the IDFs of PI for the above cases. The order of increasing dampening effects on the waves due to the stenosis effect for the given cases changes here surprisingly, which can be seen in the Figure 45 by comparing it with Figure 43 and 44. Due to the dual stenoses, behavior of the variation also looks different compared to that in the case of the single stenosis.

Long stenoses

Finally, the effect of a very long stenosis has been studied. A 0.1 meter long stenosis has been introduced in the radial artery, and also in both the brachial and radial arteries at the same time.

FIGURE 43. Pressure waves at the distal end of the artery for the control case and for the cases of
(a) a 75% stenosis in the brachial artery and a 75% stenosis in the radial artery
(b) a 50% stenosis in the brachial artery and a 90% stenosis in the radial artery
(c) a 75% stenosis in the brachial artery and a 90% stenosis in the radial artery
(d) a 90% stenosis in the brachial artery and a 50% stenosis in the radial artery
(e) a 90% stenosis in the brachial artery and a 75% stenosis in the radial artery
(f) a 90% stenosis in the brachial artery and a 90% stenosis in the radial artery

FIGURE 44. Flow waves at the distal end of the artery for the control case and for the cases of
(a) a 75% stenosis in the brachial artery and a 75% stenosis in the radial artery
(b) a 50% stenosis in the brachial artery and a 90% stenosis in the radial artery
(c) a 75% stenosis in the brachial artery and a 90% stenosis in the radial artery
(d) a 90% stenosis in the brachial artery and a 50% stenosis in the radial artery
(e) a 90% stenosis in the brachial artery and a 75% stenosis in the radial artery
(f) a 90% stenosis in the brachial artery and a 90% stenosis in the radial artery

FIGURE 45. Inverse Damping Factors of the Pulsatility Indices for the control case and for the cases of
(a) a 75% stenosis in the brachial artery and a 75% stenosis in the radial artery
(b) a 50% stenosis in the brachial artery and a 90% stenosis in the radial artery
(c) a 75% stenosis in the brachial artery and a 90% stenosis in the radial artery
(d) a 90% stenosis in the brachial artery and a 50% stenosis in the radial artery
(e) a 90% stenosis in the brachial artery and a 75% stenosis in the radial artery
(f) a 90% stenosis in the brachial artery and a 90% stenosis in the radial artery

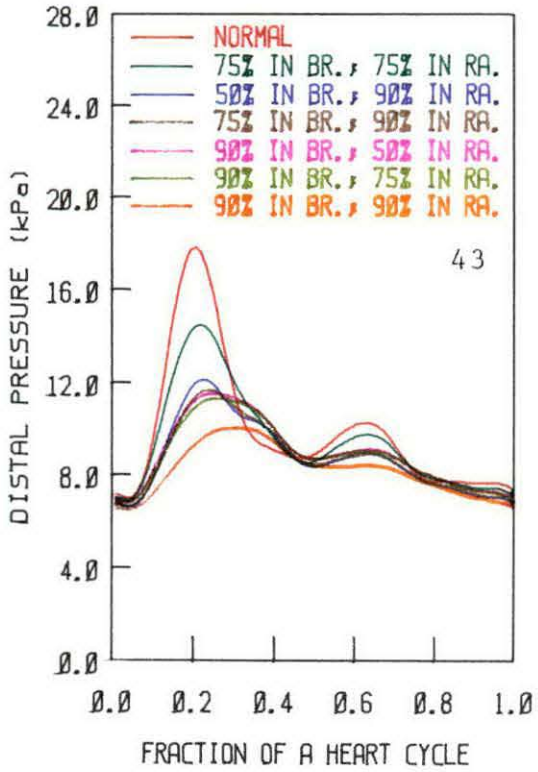
NORMAL
75% IN BR.; 75% IN RA.
50% IN BR.; 90% IN RA.
75% IN BR.; 90% IN RA.
90% IN BR.; 50% IN RA.
90% IN BR.; 75% IN RA.
90% IN BR.; 90% IN RA.
43
DISTAL PRESSURE (kPa)
28.0
24.0
20.0
16.0
12.0
8.0
4.0
0.0
0.0
0.2
0.4
0.6
0.8
1.0
FRACTION OF A HEART CYCLE

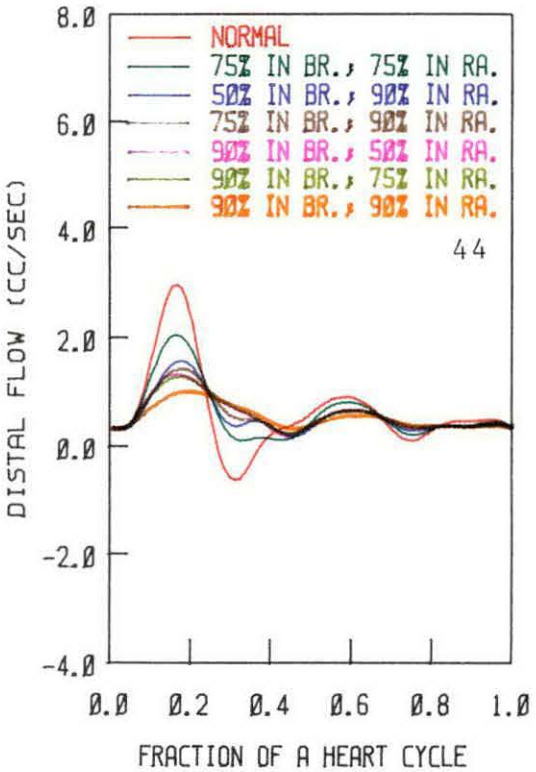
NORMAL
75% IN BR.; 75% IN RA.
50% IN BR.; 90% IN RA.
75% IN BR.; 90% IN RA.
90% IN BR.; 50% IN RA.
90% IN BR.; 75% IN RA.
90% IN BR.; 90% IN RA.
44
DISTAL FLOW (CC/SEC)
8.0
6.0
4.0
2.0
0.0
-2.0
-4.0
0.0
0.2
0.4
0.6
0.8
1.0
FRACTION OF A HEART CYCLE

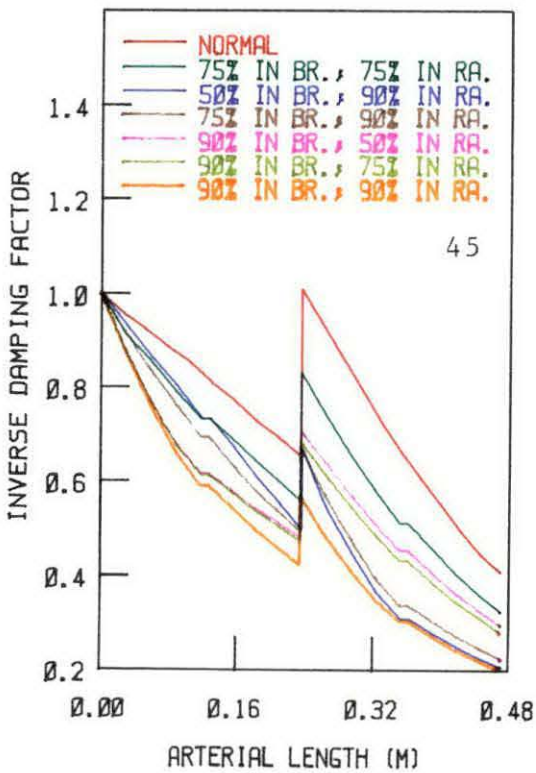
NORMAL
75% IN BR.; 75% IN RA.
50% IN BR.; 90% IN RA.
75% IN BR.; 90% IN RA.
90% IN BR.; 50% IN RA.
90% IN BR.; 75% IN RA.
90% IN BR.; 90% IN RA.
45
INVERSE DAMPING FACTOR
1.4
1.2
1.0
0.8
0.6
0.4
0.2
0.00
0.16
0.32
0.48
ARTERIAL LENGTH (M)

FIGURE 46. Pressure waves at the distal end of the artery for the control case and for the cases of placing 0.1 m long stenosis in the radial artery as follows:
(a) a 0% stenosis in the brachial artery and a 50% stenosis in the radial artery
(b) a 0% stenosis in the brachial artery and a 75% stenosis in the radial artery
(c) a 0% stenosis in the brachial artery and a 90% stenosis in the radial artery

FIGURE 47. Flow waves at the distal end of the artery for the control case and for the cases of placing 0.1 m long stenosis in the radial artery as follows:
(a) a 0% stenosis in the brachial artery and a 50% stenosis in the radial artery
(b) a 0% stenosis in the brachial artery and a 75% stenosis in the radial artery
(c) a 0% stenosis in the brachial artery and a 90% stenosis in the radial artery

FIGURE 48. Inverse Damping Factors of the Pulsatility Indices for the control case and for the cases of placing 0.1 m long stenoses in the radial artery as follows:
(a) a 0% stenosis in the brachial artery and a 50% stenosis in the radial artery
(b) a 0% stenosis in the brachial artery and a 75% stenosis in the radial artery
(c) a 0% stenosis in the brachial artery and a 90% stenosis in the radial artery

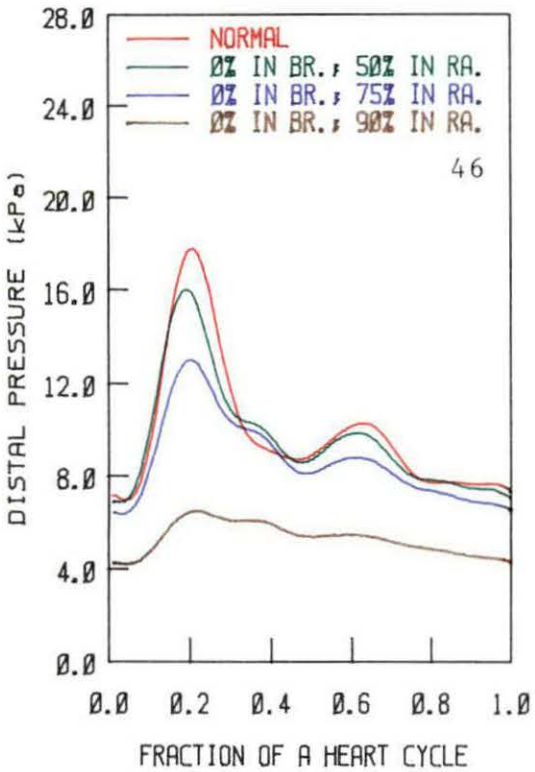
NORMAL
0% IN BR.; 50% IN RA.
0% IN BR.; 75% IN RA.
0% IN BR.; 90% IN RA.
46
DISTAL PRESSURE (kPa)
28.0
24.0
20.0
16.0
12.0
8.0
4.0
0.0
0.0
0.2
0.4
0.6
0.8
1.0
FRACTION OF A HEART CYCLE

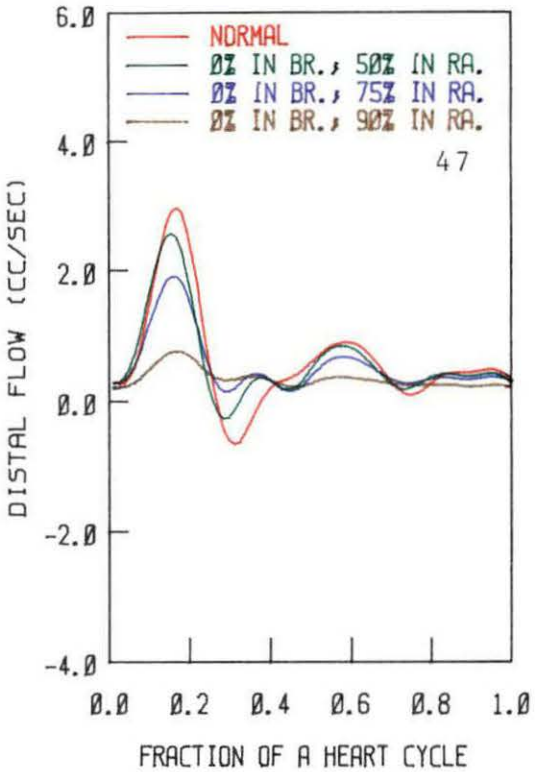
NORMAL
0% IN BR.; 50% IN RA.
0% IN BR.; 75% IN RA.
0% IN BR.; 90% IN RA.
47
DISTAL FLOW (CC/SEC)
6.0
4.0
2.0
0.0
-2.0
-4.0
0.0
0.2
0.4
0.6
0.8
1.0
FRACTION OF A HEART CYCLE

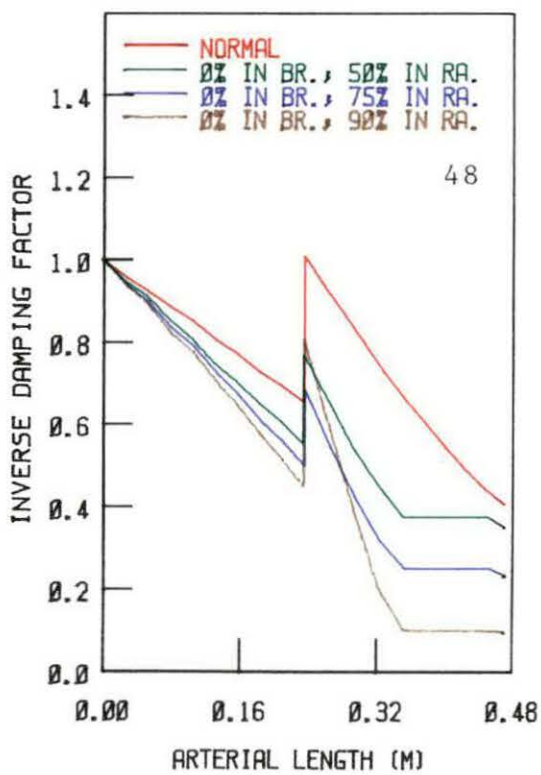
NORMAL
0% IN BR.; 50% IN RA.
0% IN BR.; 75% IN RA.
0% IN BR.; 90% IN RA.
48
INVERSE DAMPING FACTOR
1.4
1.2
1.0
0.8
0.6
0.4
0.2
0.0
0.00
0.16
0.32
0.48
ARTERIAL LENGTH (M)

FIGURE 49. Pressure waves at the distal end of the artery for the control case and for the cases of placing 0.1 m long stenosis in both the brachial and radial arteries at the same time as follows:
(a) a 75% stenosis in the brachial artery and a 75% stenosis in the radial artery
(b) a 90% stenosis in the brachial artery and a 50% stenosis in the radial artery
(c) a 50% stenosis in the brachial artery and a 90% stenosis in the radial artery
(d) a 90% stenosis in the brachial artery and a 90% stenosis in the radial artery

FIGURE 50. Flow waves at the distal end of the artery for the control case and for the cases of placing 0.1 m long stenosis in both the brachial and radial arteries at the same time as follows:
(a) a 75% stenosis in the brachial artery and a 75% stenosis in the radial artery
(b) a 90% stenosis in the brachial artery and a 50% stenosis in the radial artery
(c) a 50% stenosis in the brachial artery and a 90% stenosis in the radial artery
(d) a 90% stenosis in the brachial artery and a 90% stenosis in the radial artery

FIGURE 51. Inverse Damping Factors of the Pulsatility Indices for the control case and for the cases of placing 0.1 m long stenosis in both the brachial and radial arteries at the same time as follows:
(a) a 75% stenosis in the brachial artery and a 75% stenosis in the radial artery
(b) a 90% stenosis in the brachial artery and a 50% stenosis in the radial artery
(c) a 50% stenosis in the brachial artery and a 90% stenosis in the radial artery
(d) a 90% stenosis in the brachial artery and a 90% stenosis in the radial artery

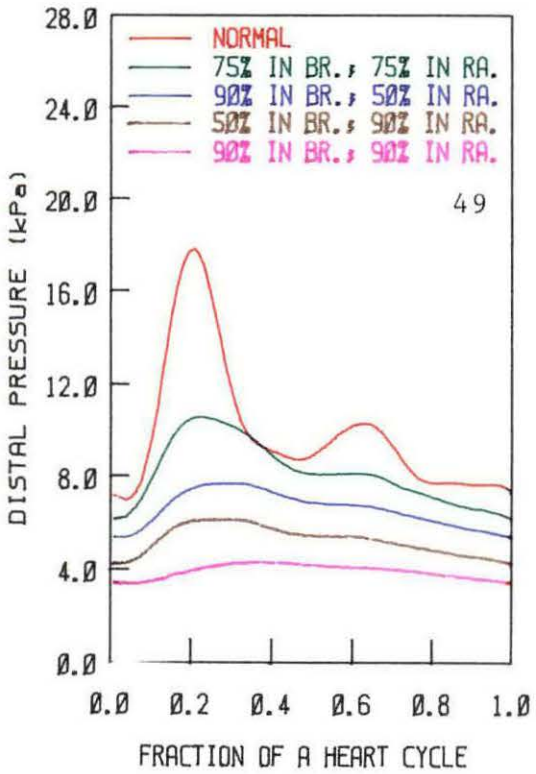
NORMAL
75% IN BR.; 75% IN RA.
90% IN BR.; 50% IN RA.
50% IN BR.; 90% IN RA.
90% IN BR.; 90% IN RA.
49
DISTAL PRESSURE (kPa)
28.0
24.0
20.0
16.0
12.0
8.0
4.0
0.0
0.0
0.2
0.4
0.6
0.8
1.0
FRACTION OF A HEART CYCLE

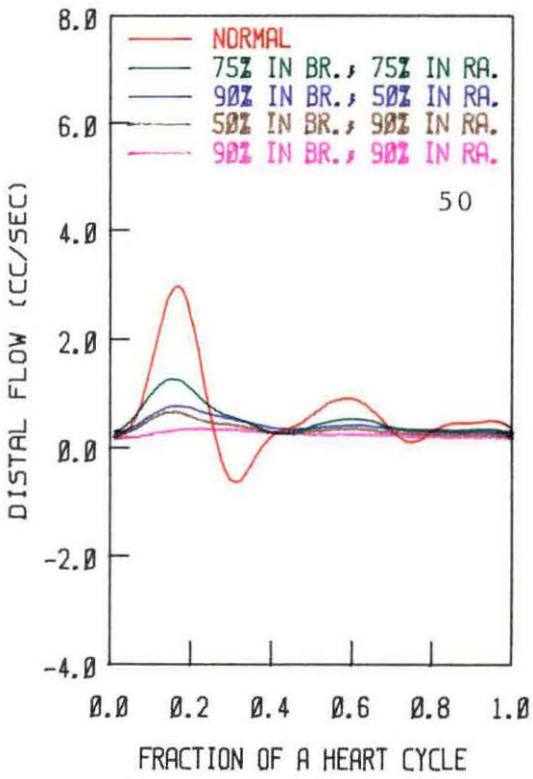
NORMAL
75% IN BR.; 75% IN RA.
90% IN BR.; 50% IN RA.
50% IN BR.; 90% IN RA.
90% IN BR.; 90% IN RA.
50
DISTAL FLOW (CC/SEC)
8.0
6.0
4.0
2.0
0.0
-2.0
-4.0
0.0
0.2
0.4
0.6
0.8
1.0
FRACTION OF A HEART CYCLE

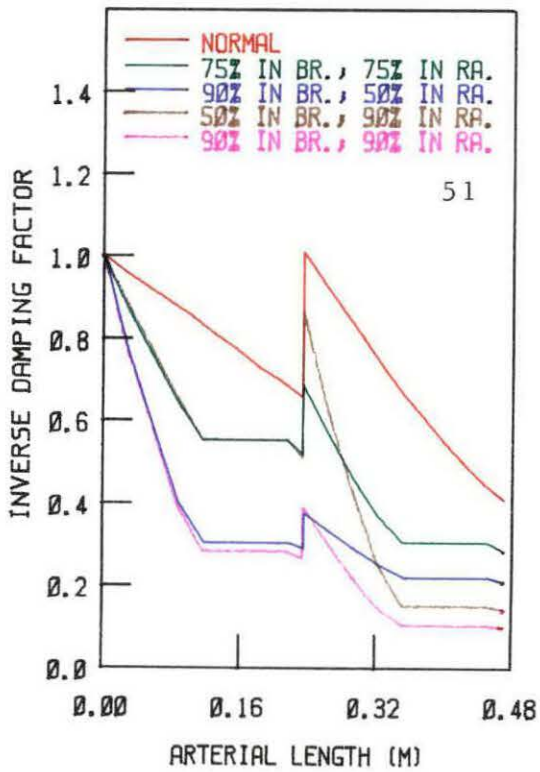
NORMAL
75% IN BR.; 75% IN RA.
90% IN BR.; 50% IN RA.
50% IN BR.; 90% IN RA.
90% IN BR.; 90% IN RA.
51
INVERSE DAMPING FACTOR
1.4
1.2
1.0
0.8
0.6
0.4
0.2
0.0
0.00
0.16
0.32
0.48
ARTERIAL LENGTH (M)

Figures 46 and 47 show the comparison of distal pressure and distal flow, respectively, when the 0.1 m long stenosis was introduced beginning at the center of the radial artery. The effect of dampening of the waves are much more severe compared to that of 0.01 m long stenosis. Figure 48 shows the IDFs of PI for the same case. Here, the values of IDFs drop very rapidly, and the value of IDF at the distal end is much lower compared to that in the case of 0.01 m long stenosis.

Figures 49 and 50 represent the case of a dual stenosis each having length of 0.1 m, placed in a similar fashion in both arteries. The effects are very severe here. Pressure and flow waves are damped out drastically. Figure 51 shows the behavior of the IDFs with a long stenosis in both arteries.

Effects of Changes in C_0 and C_1

Figures 52, 53 and 54 show the results of changing the values of the linear compliance term C_0 and the nonlinear compliance term C_1 by factor of 1.5, 1.25, 0.75 and 0.5, respectively. The reduction of the values of C_0 and C_1 was found to decrease the systolic pressure and increase the diastolic pressure, and vice versa (Figure 52).

The terms C_0 and C_1 are approximately inversely proportional to the square and fourth power of a_0, and a_0 is directly proportional to E (refer to the equation (10)). Thus, a decrease in the values of C_0 and C_1 increase the value of a_0, and subsequently the value of E is increased. The increase in elasticity makes the tube stiffer, and

FIGURE 52. Pressure waves at the distal end of the artery for the control case and for the cases of
(a) $C_0 = 1.5C_0$ and $C_1 = 1.5C_1$
(b) $C_0 = 1.25C_0$ and $C_1 = 1.25C_1$
(C) $C_0 = 0.75C_0$ and $C_1 = 0.75C_1$
(d) $C_0 = 0.5C_0$ and $C_1 = 0.5C_1$

FIGURE 53. Flow waves at the distal end of the artery for the control case and for the cases of
(a) $C_0 = 1.5C_0$ and $C_1 = 1.5C_1$
(b) $C_0 = 1.25C_0$ and $C_1 = 1.25C_1$
(c) $C_0 = 0.75C_0$ and $C_1 = 0.75C_1$
(d) $C_0 = 0.5C_0$ and $C_1 = 0.5C_1$

FIGURE 54. Inverse Damping Factors of the Pulsatility Indices for the control case and for the cases of
(a) $C_0 = 1.5C_0$ and $C_1 = 1.5C_1$
(b) $C_0 = 1.25C_0$ and $C_1 = 1.25C_1$
(c) $C_0 = 0.75C_0$ and $C_1 = 0.75C_1$
(d) $C_0 = 0.5C_0$ and $C_1 = 0.5C_1$

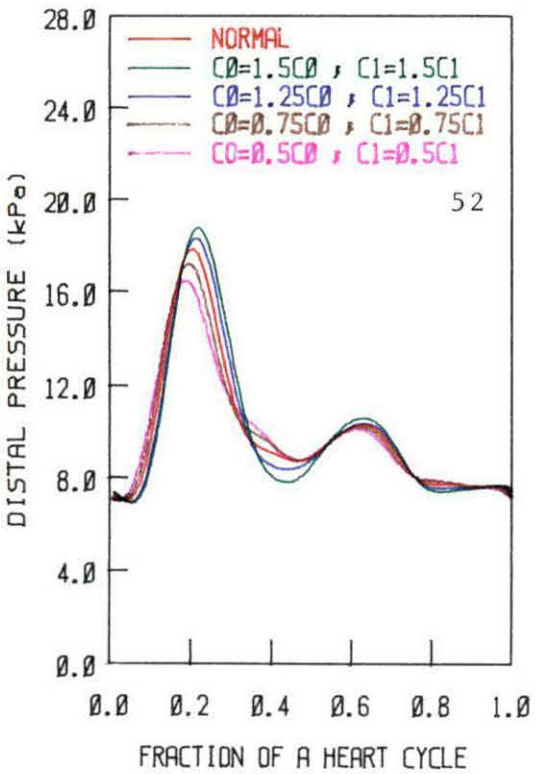
NORMAL
C0=1.5C0 , C1=1.5C1
C0=1.25C0 , C1=1.25C1
C0=0.75C0 , C1=0.75C1
C0=0.5C0 , C1=0.5C1
52
DISTAL PRESSURE (kPa)
28.0
24.0
20.0
16.0
12.0
8.0
4.0
0.0
0.0
0.2
0.4
0.6
0.8
1.0
FRACTION OF A HEART CYCLE

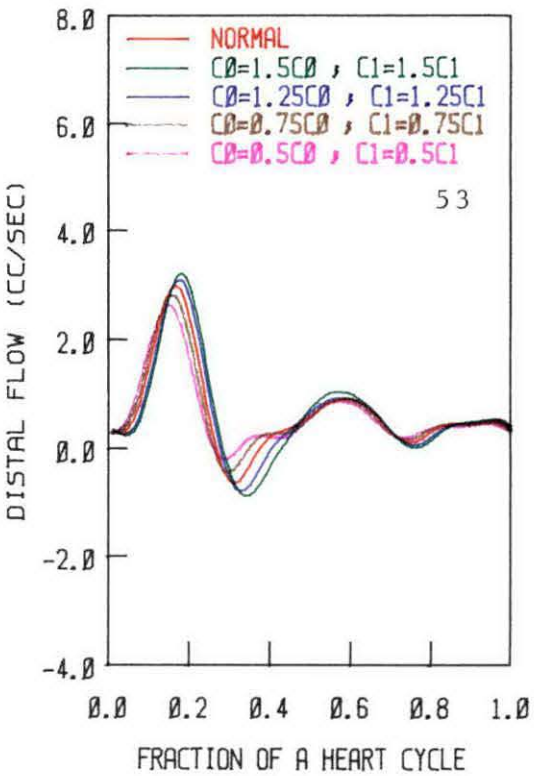
NORMAL
C0=1.5C0 , C1=1.5C1
C0=1.25C0 , C1=1.25C1
C0=0.75C0 , C1=0.75C1
C0=0.5C0 , C1=0.5C1
53
DISTAL FLOW (CC/SEC)
8.0
6.0
4.0
2.0
0.0
-2.0
-4.0
0.0
0.2
0.4
0.6
0.8
1.0
FRACTION OF A HEART CYCLE

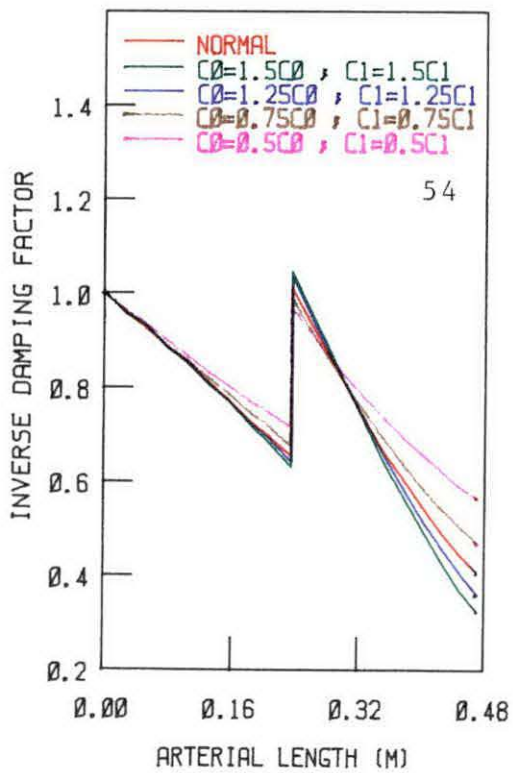
NORMAL
C0=1.5C0 , C1=1.5C1
C0=1.25C0 , C1=1.25C1
C0=0.75C0 , C1=0.75C1
C0=0.5C0 , C1=0.5C1
54
INVERSE DAMPING FACTOR
1.4
1.2
1.0
0.8
0.6
0.4
0.2
0.00
0.16
0.32
0.48
ARTERIAL LENGTH (M)

it causes a decrease in systolic pressure. The effect is reversed, when the values of C_0 and C_1 are increased. Since arteriosclerosis causes the arterial wall to become less compliant, either by calcification or by thickening of the tissue, this is an important effect to be studied with a computer model (Raines et al., 1974). Gribbin et al. (1979) reported that poor distensibility of large arteries in hypertensive subjects is a consequence of the elevated distending pressure; however, Randall et al. (1984) mentioned that changes in arterial compliance alone cannot explain isolated systolic hypertension. Simon et al. (1983) reported that the reduced forearm compliance in hypertension is independent of blood pressure, but may reflect adaptive changes in the walls of the large arteries. Apart from these research studies, there was an interesting case of a patient (reported by Taguchi and Suwangool, 1974), which proved importance of arterial compliance in blood pressure measurement. The brachial arterial wall of that patient was so severely calcified that the cuff could not compress the arteries, and the patient was reported to be a case of artifactual hypertension. The recorded blood pressure exceeded 300 mm Hg in both arms even though the real blood pressure was much lower. All above studies indicate the importance of studying the effect of arterial compliance on hemodynamic parameters.

Figure 53 shows the results of changing C_0 and C_1 on the flow, and changes in flow appear to be similar to the changes in the pressure. The IDFs of pulsatility indices at the distal end of the artery decrease with increase in values of C_0 and C_1 (Figure 54).

Effects of Changes in Lumped Resistances

Figures 55 and 56 show the pressure and flow waveforms, respectively, for the case in which the resistance of the lumped ends is reduced by factor of 5. The pressure reduces, while the flow elevates significantly by dilating the lumped resistance. The flow waveform of Figure 56 is represented differently (Figure 58) by repeating the same cycles again and again in a scale suitable to compare them with the actual recordings shown in Figures 59, 60, 61 and 62. The actual recordings were measured for the purpose of verifying the results obtained by the computer. The actual recordings were measured for three different subjects whose data are entered in the Table 7. An ultrasonic strip chart recorder was used to measure the flow waveforms by placing the probe on the radial artery of the subjects mentioned in Table 7. The flow waveforms obtained by the computer (Figure 58) match closely with the actual recordings shown in Figures 59 to 62. One can notice differences in the flow

TABLE 7. Data for the three human subjects whose flow recordings were measured

Subjects (Sr No.)	Sex	Age (Years)	Weight (Kg)	Height (cm)	Physiological condition
1	Male	27	75	193	Healthy (without any disease)
2	Male	49	78	168	Healthy (without any disease)
3	Male	57	80	180	Healthy (without any disease)

FIGURE 55. Pressure waves at the distal end of the artery for the control case and the case when both the lumped resistances are reduced by a factor of 5

FIGURE 56. Pressure waves at the distal end of the artery for the control case and the case when both the lumped resistances are reduced by a factor of 5

FIGURE 57. Inverse Damping Factors at the distal end of the artery for the control case and the case when both the lumped resistances are reduced by a factor of 5

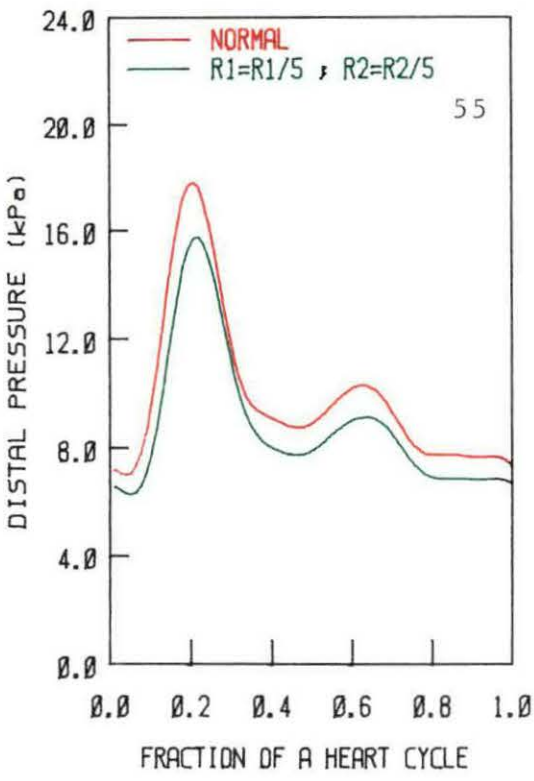
NORMAL
R1=R1/5 ; R2=R2/5
55
DISTAL PRESSURE (kPa)
24.0
20.0
16.0
12.0
8.0
4.0
0.0
0.0
0.2
0.4
0.6
0.8
1.0
FRACTION OF A HEART CYCLE

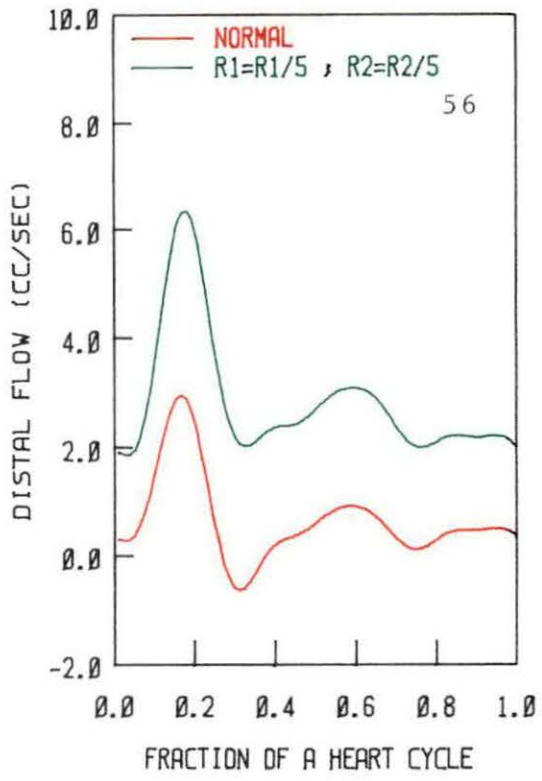
NORMAL
R1=R1/5 ; R2=R2/5
56
DISTAL FLOW (CC/SEC)
10.0
8.0
6.0
4.0
2.0
0.0
-2.0
0.0
0.2
0.4
0.6
0.8
1.0
FRACTION OF A HEART CYCLE

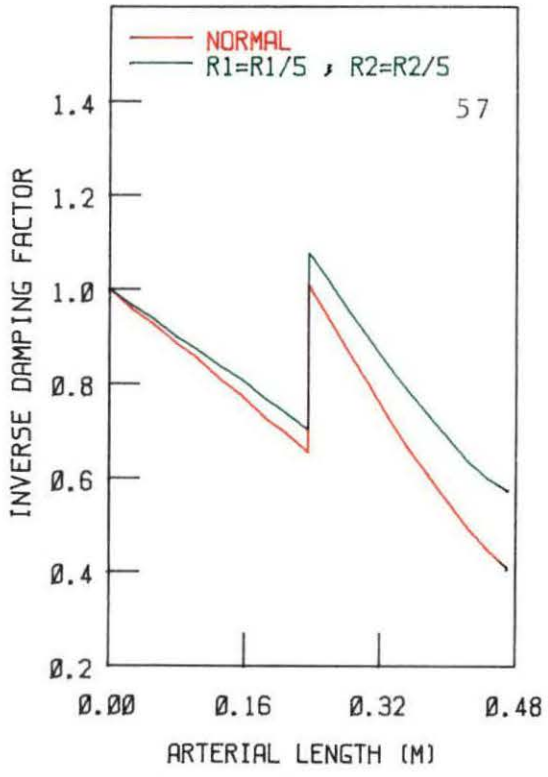
NORMAL
R1=R1/5 ; R2=R2/5
57
INVERSE DAMPING FACTOR
1.4
1.2
1.0
0.8
0.6
0.4
0.2
0.00
0.16
0.32
0.48
ARTERIAL LENGTH (M)

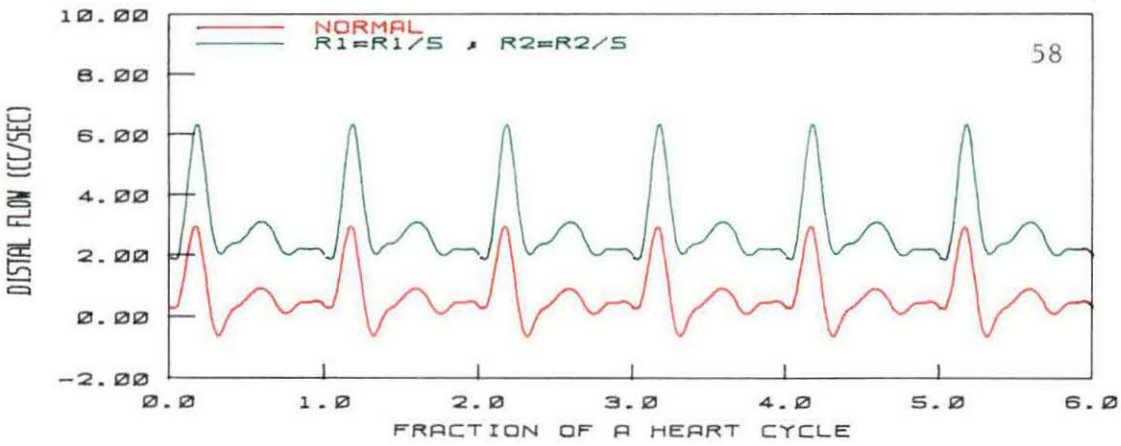
NORMAL
R1=R1/5 , R2=R2/5
58
10.00
8.00
6.00
4.00
2.00
0.00
-2.00
DISTAL FLOW (CC/SEC)
0.0
1.0
2.0
3.0
4.0
5.0
6.0
FRACTION OF A HEART CYCLE

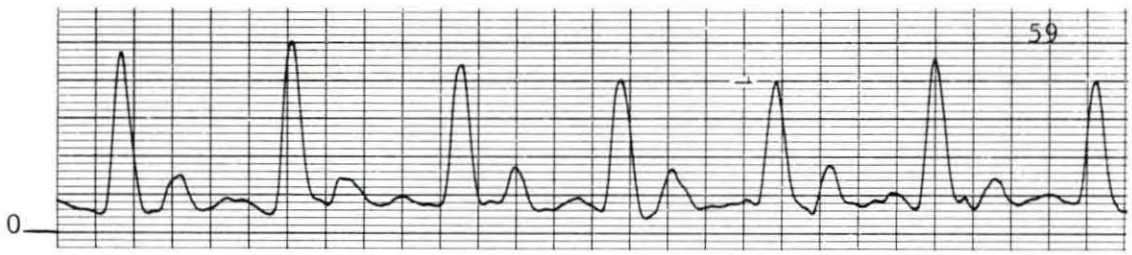
59
0

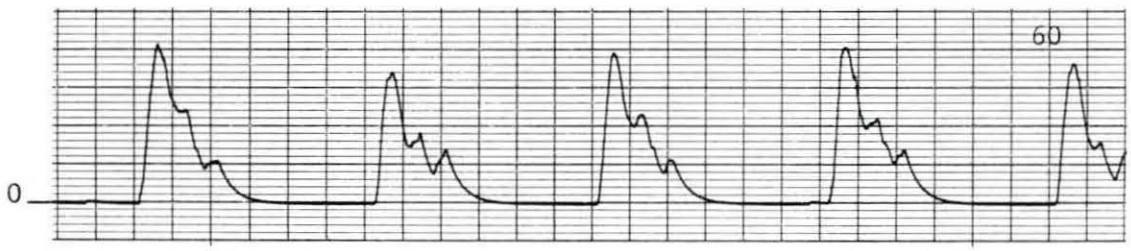
60
0

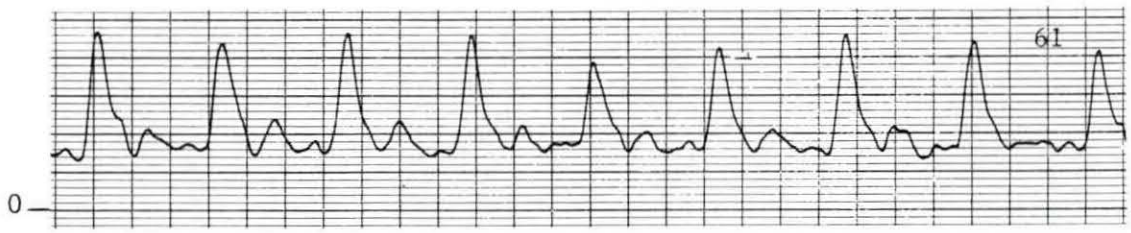
61
0

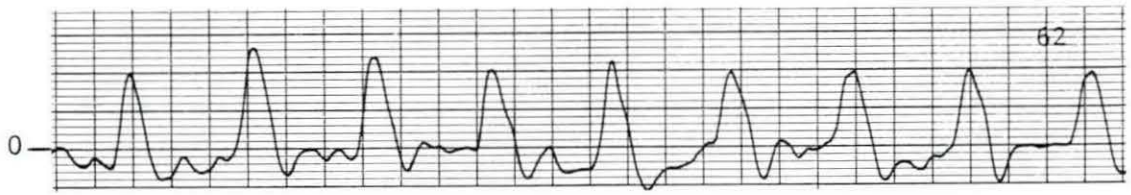
62
0

patterns among the Figures 59, 60 and 61. The time period for the Figure 60 is much longer compared to the other two cases. That means the heart rate of the subject 2 should be lower. That indicates that the subject's heart delivers more blood per beat, and probably the subject's athletic condition should be better. Comparisons of Figures 59 and 61 indicate that the peak flow is more elevated for the subject 1 compared to that of the subject 3. The recording in Figures 61 and 62 are for the same subject, but in different conditions. Figure 61 indicates a normal flow recording while Figure 62 shows the recorded flow when the fist of the subject 3 was closed. The closing of the fist resulted in an increase of the resistance, which caused a decrease in flow. When the fist was opened again, the flow was suddenly elevated, and then became normal. Opening of the fist dilates the resistance of the flow, and hence an increase in flow takes place. This phenomenon was verified by the computer result, which was discussed earlier and shown in Figure 58. In clinical situations, abrupt changes in the flow may be caused by the changes in resistances, and the present study provides some insight relative to the effect of these changes. Another parameter which may be useful in that situation is the IDF. Figure 57 shows the comparison of IDFs of PI for the normal arteries as well as the arteries with dilated resistance. The IDFs are higher in arteries with reduced resistances.

The present work may be indirectly verified by Raines et al.'s (1974) work. In their study, a distal cuff was used on the foot to increase the resistance of the flow. A subject's foot was placed in

iced water to cause vasoconstriction, and in hot water to cause vasodilation. Vasoconstriction was used to verify the effects of a decrease in the resistance of flow, while vasodilation was used to verify the effects of a decrease in the resistance of flow. Raines et al. (1974) have studied the effect on the changes in pressure, while in the present study the effect on the change in flow was of a prime interest.

SUMMARY

An extensive literature survey was done to know the physiological significance of studying blood flow in human arteries and to collect the required data needed for model in arteries.

A mathematical model of blood flow in the arteries in a human arm has been developed based on three equations: the continuity equation, the momentum equation, and an equation of state for the artery. A linear taper was considered for the model geometry. The finite element method was used to simulate blood flow on a high-speed digital computer.

A physiological model was prepared showing the required arterial dimensions and flow distributions. Necessary calculations were carried out along with corresponding plots.

Results representing pressure waveforms, flow waveforms and inverse damping factor curves were obtained for a control case and various disease conditions of the brachial and radial arteries, and are summarized in Table 8. Several different diseased cases were considered, including: hypertension, aortic valvular stenosis, pure aortic regurgitation, and combined aortic stenosis and regurgitation. Also included were the cases of stenoses of various lengths and different combinations in the brachial and radial arteries, increased and reduced values of C_0 and C_1, and reduced resistances.

The present study may be useful for the development of a clinically important

TABLE 8. Details of control case and various diseased conditions of brachial and radial arteries

Sr. No.	Percent Stenoses in Brachial Artery	Percent Stenoses in Radial Artery	Length of Stenoses (meter)	Compliance	Resistance
1.	0 (Control case)	0	0	normal	normal
2.	50	0	0.1E-1	normal	normal
3.	75	0	0.1E-1	normal	normal
4.	90	0	0.1E-1	normal	normal
5.	0	50	0.1E-1	normal	normal
6.	0	75	0.1E-1	normal	normal
7.	0	90	0.1E-1	normal	normal
8.	75	75	0.1E-1	normal	normal
9.	90	90	0.1E-1	normal	normal
10.	50	90	0.1E-1	normal	normal
11.	90	50	0.1E-1	normal	normal
12.	75	90	0.1E-1	normal	normal
13.	90	75	0.1E-1	normal	normal
14.	0	50	0.1E00	normal	normal
15.	0	75	0.1E00	normal	normal
16.	0	90	0.1E00	normal	normal
17.	75	75	0.1E00	normal	normal
18.	90	90	0.1E00	normal	normal
19.	50	90	0.1E00	normal	normal
20.	90	50	0.1E00	normal	normal
21.	0	0	0	$C_0=0.50C_0$, $C_1=0.50C_1$	normal
22.	0	0	0	$C_0=0.75C_0$, $C_1=0.75C_1$	normal
23.	0	0	0	$C_0=1.25C_0$, $C_1=1.25C_1$	normal
24.	0	0	0	$C_0=1.50C_0$, $C_1=1.50C_1$	normal
25.	0	0	0	normal	$R_1=R_1/5$, $R_2=R_2/5$
26.	0 (Hypertension)	0	0	normal	normal
27.	0 (Diseased heart pulse with AS)	0	0	normal	normal
28.	0 (Diseased heart pulse with AI)	0	0	normal	normal
29.	0 (Diseased heart pulse with AS/AI)	0	0	normal	normal

noninvasive diagnostic tool, and may be used to distinguish the variation in various hemodynamic parameters and waveforms of a normal person from a diseased person. It can be useful to fill the gap between the results of in vivo and in vitro experiments by analysing various waveforms when the system parameters are varied. Also, the study of a simple arm model like this may give better insight into the corresponding behavior of flow characteristics in other vessels such as the carotid artery and the coronary artery.

BIBLIOGRAPHY

Andres, R., K. L. Zierler, H. M. Anderson, W. N. Stainsby, G. Cader, A. S. Ghrayyib, and J. L. Lilienthal, Jr. 1954. Measurement of blood flow and volume in the forearm of man; with notes on the theory of indicator-dilution and on production of turbulence, hemolysis, and vasodilation by intra-vascular injection. Journal of Clinical Investigation 33:482-504.

Avolio, A. P. 1980. Multi-branched model of the human arterial system. Medical and Biological Engineering and Computing 18:709-718.

Avolio, A. P., S. Chen, R. Wang, C. Zhang, M. Li, and M. F. O'Rourke. 1983. Effects of aging on changing arterial compliance and left ventricular load in a northern Chinese urban community. Circulation 68(1):50-58.

Barnes, R. W., J. L. Petersen, R. B. Krugmire, and D. Strandness. 1974. Complications of brachial artery catheterization: Prospective evaluation with the doppler ultrasonic velocity detector. Chest 66(4):363-367.

Bennett, D., P. Winter, and S. Moss. 1980. Non-invasive measurement of brachial artery peak velocity as an index of cardiac performance in normal subjects and patients with acute myocardial infection. Clinical Science 58(2):11p.

Caro, C. G., T. H. Foley, and M. F. Sudlow. 1968. Early effects of abrupt reduction on local pressure on the forearm and its circulation. Journal of Physiology 194:645-658.

Clark, M. E., F. H. Erdman, R. H. Kufahl, and W. D. Ulrich. 1985. Upper extremity arterial flow simulation. Pp. 95-98. Morton H. Friedman and David C. Wiggert, eds. Forum on unsteady flows in biological systems. ASME, New York.

Doupe, J., H. W. Newman, and R. W. Wilkins. 1939. The effect of peripheral vasomotor activity on systolic arterial pressure in the extremities of man. Journal of Physiology 95:244-257.

Ewy, G. A., J. C. Rios, and F. I. Marcus. 1969. The dicrotic arterial pulse. Circulation 39:655-661.

Fitchett, D. H. 1984. Forearm arterial compliance: A new measure of arterial compliance? Cardiovascular Research 18:651-656.

Floras, J. S., J. V. Jones, M. O. Hassan, B. Osikowska, P. S. Sever, and P. Sleight. 1981. Cuff and ambulatory blood pressure in subjects with essential hypertension. Lancet 2(8238):107-109.

Foley, T. H., and J. L. Greenberg. 1969. Early changes in the forearm circulation following transient increase of local external pressure. Journal of Physiology 203:111-119.

Fulton, J. S., and B. A. McSwiney. 1925. The pulse wave velocity and extensibility of the brachial and radial artery in man. Journal of Physiology (London) 69:386-392.

Gaskell, P., and A. M. Krisman. 1958. The brachial to digital blood pressure gradient in normal subjects and in patients with high blood pressure. Canadian Journal of Biochemistry and Physiology 36:889-893.

Gault, J. H., J. Ross, and D. T. Mason. 1966. Patterns of brachial arterial blood flow in conscious human subjects with and without cardiac dysfunction. Circulation 34:833-48.

Geddes, L. A., M. H. Voelz, C. F. Babbs, J. D. Bourland, and W. A. Tacker. 1981. Pulse transit time as an indicator of arterial blood pressure. Psychophysiology 18:71-74.

Giuliani, M. G., and L. Gould. 1969. The pitfalls of the brachial arterial pressure curve in the evaluation of valvular aortic stenosis. Japanese Heart Journal 10(5):467-473.

Gribbin, B., A. Steptoe, and P. Sleight. 1976. Pulse wave velocity as a measure of blood pressure change. Psychophysiology 13:86-90.

Gribbin, B., T. G. Pickering, and P. Sleight. 1979. Arterial distensibility in normal and hypertensive man. Clinical Science 56:413-417.

Hamilton, W. F., R. A. Woodbury, and H. T. Harper. 1936. Physiologic relationships between intrathoracis, intraspinal and arterial pressures. Journal of the American Medical Association 107(11):853-856.

Hancock, E. W., and W. H. Abelmann. 1957. A clinical study of the brachial arterial pulse form with special reference to the diagnosis of aortic valvular disease. Circulation 16:572-581.

Hawker, R. E., C. A. Seara, and L. J. Krovetz. 1974. Distalward modification of the arterial pulse wave in children with congenital aortic stenosis. Circulation 50:181-187.

Helps, E. P. W., and D. A. McDonald. 1953. Systolic backflow in the dog femoral artery. Journal of Physiology 122:73p.

Helps, E. P. W., and D. A. McDonald. 1954. Arterial blood flow calculated from pressure gradient. Journal of Physiology 124:30p-31p.

Inagaki, Y. I., M. Wassermil, and S. Rodbard. 1976. Effects of treadmill exercise on the timing of the brachial arterial pulse wave. American Heart Journal 92:283-289.

Kannel, W. B., P. A. Wolf, D. L. McGee, T. R. Dawber, P. McNamara, and W. P. Castelli. 1981. Systolic blood pressure, arterial rigidity, and risk of stroke (the Framingham study). Journal of the American Medical Association 245(12):1225-1229.

Karwash, S. G., J. E. Jacobs, and L. F. Mockros. 1979. Disease diagnosis from arterial pressure waveforms. Proceedings Third Engineering Mechanics 1979:582-585.

Kato, M., T. Koeda, H. Inomata, A. Motoyama, K. Nakai, T. Kimura, and T. Chiba. 1977. Measurement of digital arterial blood pressure and its recording on usual electrocardiograph paper. Tohoku Journal of Experimental Medicine 123:307-314.

Kerslake, D. Mck. 1949. The effect of the application of an arterial occlusion cuff to the wrist on the blood flow in the human forearm. Journal of Physiology 108:451-457.

Kroeker, E. J., and E. H. Wood. 1955. Comparison of simultaneously recorded central and peripheral arterial pressure pulses during rest, exercise and tilted position in man. Circulation Research 3:623-632.

Kroeker, E. J., and E. H. Wood. 1956. Beat-to-beat alterations in relationship of simultaneously recorded central and peripheral arterial pressure pulses during valsalva maneuver and prolonged expiration in man. Journal of Applied Physiology 8:483-494.

Levenson, J. A., P. A. Peronneau, A. Simon, and M. E. Safar. 1981. Pulsed doppler: Determination of diameter, blood flow velocity, and volumic flow of brachial artery in man. Cardiovascular Research 15:164-170.

Mason, D. T., E. Braunwald, J. Ross, and A. G. Morrow. 1964. Diagnostic value of the first and second derivatives of the arterial pressure pulse in aortic valve disease and in hypertrophic subaortic stenosis. Circulation 30:90-100.

McDonald, D. A. 1952. The velocity of blood flow in the rabbit aorta studied with high-speed cinematography. Journal of Physiology 118:328-339.

McDonald, D. A. 1955. The relationship of pulsatile pressure to flow in arteries. Journal of Physiology 127:533-552.

McDonald, D. A. 1974. Blood flow in arteries. Edward Arnold, London.

Millington, P. F., and P. Record. 1977. Measurement of the radial arterial pulse under clinical conditions. Journal of Physiology 273: 46p-47p.

Nakayama, R., and T. Azuma. 1977. Noninvasive measurements of digital arterial pressure and compliance in man. American Journal of Physiology 233(1):H168-H179.

Noordergraf, A., G. N. Jager, and N. Westerhof. 1963. Circulatory analog computers. North-Holland Publishing, Amsterdam.

Obrist, P. A., K. C. Light, J. A. McCubbin, J. S. Hutcheson, and J. L. Hoffer. 1979. Pulse transit time: Relationship to blood pressure and myocardial performance. Psychophysiology 16:292-301.

O'Rourke, M. F. 1970. Influence of ventricular ejection on the relationship between central aortic and brachial pressure pulse in man. Cardiovascular Research 4:291-300.

O'Rourke, M. F. 1971. The arterial pulse in health and disease. American Heart Journal 82:687-702.

O'Rourke, M. F. 1982. Arterial function in health and disease. Churchill Livingstone, New York.

O'Rourke, M. F., J. V. Blazek, C. L., Jr. Morreels, and J. Krovetz. 1968. Pressure wave transmission along the human aorta: Changes with age and in arterial degenerative disease. Circulation Research 23:567.

Porenta, G. 1982. A Computer based feasibility analysis of assessing arterial flow using pulsatility indices. M.S. Thesis. Iowa State University, Ames, Iowa.

Raines, J. K., M. Y. Jaffrin, and A. H. Shapiro. 1974. A computer simulation of arterial dynamics in the human leg. Journal of Biomechanics 7:77-91.

Randall, O. S., G. C. Van Den Bos, and N. Westerhof. 1984. Systemic compliance: Does it play a role in the genesis of essential hypertension. Cardiovascular Research 18:455-462.

Rastelli, G. C., D. T. E. Krueger, R. H. Edegerton, W. H. Hammer, L. C. Sheppard, and R. B. Wallace. 1968. Indirect measurement of arterial blood pressure with the aid of a digital computer. The American Journal of Cardiology 22:685-690.

Safar, M. E., P. A. Peronneau, J. A. Levenson, J. A. Toto-Moukouo, and A. Ch. Simon. 1981. Pulsed doppler: Diameter, blood flow velocity and volumic flow of the brachial artery in sustained essential hypertension. Circulation 63:393-400.

Scarpello, J. H. B., T. R. P. Martin, and J. D. Ward. 1980. Ultrasound measurements of pulse-wave velocity in the peripheral arteries of diabetic subjects. Clinical Science 58:53-57.

Simon, A. Ch., S. Laurent, J. A. Levenson, J. E. Bouthier, and M. E. Safar. 1983. Estimation of forearm arterial compliance in normal and hypertensive men from simultaneous pressure and flow measurements in the brachial artery, using a pulsed doppler device and a first-order arterial model during diastole. Cardiovascular Research 17:331-338.

Smulyan, H., T. J. Csermely, S. Mookherjee, and R. A. Warner. 1983. Effect of age on arterial distensibility in asymptomatic humans. Arteriosclerosis 3:199-205.

Taguchi, J. T., and P. Suwangool. 1974. "Pipe-Stem" brachial arteries A cause of pseudohypertension. Journal of the American Medical Association 228:733.

U. S. Department of Health and Human Services. 1982. National heart, lung, and blood institute's fact book for fiscal year 1982. NIH Publication No. 83-1525.

Wallace, J. M., and E. A. Stead. 1959. Fall in pressure in radial artery during reactive hyperemia. Circulation Research 7:876-879.

Weerapulli, D. 1986. [Simulation of pulsatile flow in arteries using the finite-element method.] Ph.D. Thesis. Iowa State University, Ames, Iowa.

Wesseling, K. H. 1973. Arterial haemodynamic parameters derived from noninvasively recorded pulsewaves, using parameter estimation. Medical and Biological Engineering 11(6):724-731.

Westerhof, N., F. Bosman, C. J. De Vries, and A. Noordergraaf. 1969. Analog studies of the human systemic arterial tree. Journal of Biomechanics 2:121-143.

Westerhof, N., G. Elzinga, P. Sipkema, and G. C. van den Bos. 1977. Quantitative analysis of the arterial system and heart by means of pressure-flow relations. Pp. 403-438. Ned H. C. Hwang and Nils A. Normann, eds. Cardiovascular flow dynamics and measurements. University Park Press, Baltimore.

Womersley, J. R. 1954. Flow in the larger arteries and its relationship to the oscillating pressure. Journal of Physiology 124:31p-32p.

Womersley, J. R. 1955. Method for the calculation of velocity, rate of flow and viscous drag in arteries when the pressure gradient is known. Journal of Physiology 127:553-563.

Young, D. F. 1979. Fluid mechanics of arterial stenoses. Journal of Biomechanical Engineering 101:157-175.

Young, D. F., and F. Y. Tsai. 1973. Flow characteristics in models of arterial stenoses-II. Unsteady flow. Journal of Biomechanics 6:547-559.

Young, D. F., T. R. Rogge, T. A. Gray, and E. Rooz. 1981. Indirect evaluation of system parameters for pulsatile flow in flexible tubes. Journal of Biomechanics 14(5):339-347.

ACKNOWLEDGMENTS

I would like to thank my major professor, Dr. Thomas R. Rogge, for his gentle guidance and constant encouragement throughout my graduate work. I owe a debt of gratitude to him for his help in computer programming and in editing the thesis. I sincerely wish to give special thanks to Dr. Donald F. Young for very actively serving on my committee, for being extremely helpful in the field of arterial dynamics, and for his useful suggestions on my thesis. I am also grateful to Dr. Theodore H. Okiishi for serving on my committee and for introducing me to the field of advanced fluid mechanics.

I am greatly indebted to the Department of Biomedical Engineering for providing the financial support for my graduate study.

I owe my thanks to the Human Subjects Review Committee for approving the use of human subjects for this project.

Finally, thanks to my beloved parents Damodarbhai and Savitaben, my brother Nikhil, and my sister Sushma, whose love and encouragement have made all the difference.

APPENDIX A

Determination of the Volume V_0 of the Entire Artery

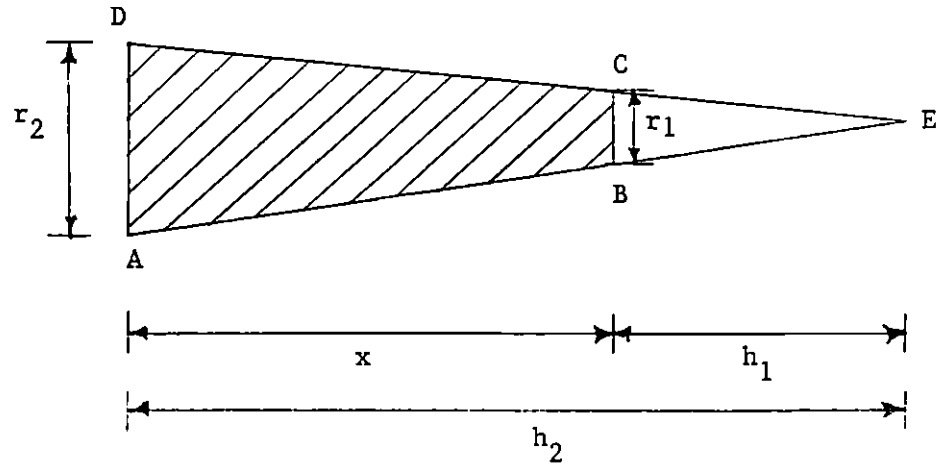

In the above figure, the area of the region BEC will be

$$V_1 = \pi/3\ r_1^2 h_1$$

and the area of the region AED will be

$$V_2 = \pi/3\ r_2^2 h_2$$

So the area of the shaded region ABCD will be

$$V = \pi/3\ [r_2^2 h_2 - r_1^2 h_1] \qquad (1)$$

Also, $h_2 = x + h_1$ (2)

So that $h_1 = h_2 - x = (r_2/r_1)h_1 - x$ [as $r_1/r_2 = h_1/h_2$]

$$h_1 = \frac{x}{\frac{r_2}{r_1} - 1} \qquad (3)$$

Volume of the brachial artery

From Westerhof et al. (1969), the dimensions of the brachial arteries are as follows:

$r_1 = 0.207$ cm, $r_2 = 0.28$ cm, $x = 23.5$ cm

Substituting these values in the equation (3), one has

$$h_1 = 66.637 \text{ cm}$$

Using the equation (2), one obtains

$$h_2 = 90.137 \text{ cm}$$

Volume of the brachial artery (by using the equation (1)),

$$V_B = 4.4102 \text{ cm}^3 = 4.4102 \times 10^{-6} \text{ m}^3$$

Volume of the radial artery

From Westerhof et al. (1969), the dimensions of the radial arteries are as follows:

$$r_1 = 0.14 \text{ cm}, \; r_2 = 0.207 \text{ cm}, \; x = 23.50 \text{ cm}$$

Volume of the radial artery is (by following the similar method as used for the brachial artery),

$$V_R = 2.2500 \text{ cm}^3 = 2.2500 \times 10^{-6} \text{ m}^3$$

Volume of the entire artery

$$V_0 = V_B + V_R = (4.4102 \times 10^{-6}) + (2.2500 \times 10^{-6})$$

$$= 6.6602 \times 10^{-6} \text{ m}^3$$

APPENDIX B

Computer Programs

```
C     ****************************************************************
C     *                                                              *
C     * THE PROGRAM TO CALCULATE MOD(K) AND THETA FOR THE PRESENT    *
C     * ARTERIAL MODEL OF THE BRACHIAL AND RADIAL ARTERIES           *
C     *                                                              *
C     ****************************************************************

C     ---------------------------------------------------------------
C     OPENING A FILE FOR CALCULATED DATA AND DECLARATION OF
C     PARAMETERS
C     ---------------------------------------------------------------
      OPEN(UNIT=13,NAME='DATA1.DAT',TYPE='NEW')
      COMPLEX ZT,Z0,Z02,RCOF
      REAL RZ02,BZ02,RZT,BZT,R,B,RMAG,X,G,W,CU,CT,RT,LU,D,PI,MU,THETA

C     ---------------------------------------------------------------
C     DEFINITION OF THE PARAMETERS USED IN THIS PROGRAM
C     ---------------------------------------------------------------
C     ZT=TERMINAL COMPLIANCE

C     Z0=LOCAL CHARACTERISTIC IMPEDANCE
C     Z02=SQUARE OF Z0
C     RZ02=REAL PART OF Z02
C     BZ02=IMAGINARY PART OF Z02
C     RZT=REAL PART OF ZT
C     BZT=IMAGINARY PART OF ZT
C     X=R1/RT WHERE R1+R2=RT
C     W=HEART FREQUENCY
C     CU=COMPLIANCE PER UNIT LENGTH
C     CT=TERMINAL COMPLIANCE
C     RT=DISTAL PERIPHERAL RESISTANCE
C     LU=INERTANCE PER UNIT LENGTH
C     D=DIAMETER OF THE VESSEL
C     MU=VISCOSITY OF THE BLOOD
C     THETA=PHASE ANGLE
C     RMAG=MOD(K) WHERE K=THE REFLECTION COEFFICIENT

C     ---------------------------------------------------------------
C     INPUT VALUES OF THE PARAMETERS
C     ---------------------------------------------------------------
      LU=0.16575E9
      CU=7.7921E-11
      W=1/0.77
      CT=0.2004E-10
```

```
      RT=0.1546E11
      D=0.0028
      PI=3.14159265
      W=2*PI*W
      N=100
      MU=0.45E-2
      RZ02=LU/CU
      BZ02=-(128*MU)/(PI*(D**4)*CU*W)
      Z02=CMPLX(RZ02,BZ02)
      Z0=CSQRT(Z02)
      RZ0=REAL(Z0)
      BZ0=AIMAG(Z0)
      WRITE (6,50)

C     ------------------------------------------------------------
C     FORMAT OF THE RESULTS
C     ------------------------------------------------------------
50    FORMAT (4X,'RZ02',12X,'BZ02',12X,'RZ0',12X,'BZ0')
      WRITE (6,100) RZ02,BZ02,RZ0,BZ0
100   FORMAT (2X,E11.4,6X,E11.4,2X,E13.4,2X,E13.4//)
      WRITE (6,200)
200   FORMAT (2X,'X=R1/RT',3X,'RMAG',2X,'THETA',4X,'RZT',12X,
     1 'BZT',12X,'R',12X,' '/)

C     ------------------------------------------------------------
C     CALCULATIONS
C     ------------------------------------------------------------
      DO 1000 I=0,N,1
      RI=FLOAT(I)
      X=RI/N
      G=1+(((1-X)**2)*(RT**2)*(CT**2)*(W**2))
      RZT=(RT*X)+((RT*(1-X)))/(G)
      BZT=-(((1-X)**2)*(RT**2)*CT*W)/(G)
      ZT=CMPLX(RZT,BZT)
      RCOF=(ZT-Z0)/(ZT+Z0)
      RMAG=CABS(RCOF)
      R=REAL(RCOF)
      B=AIMAG(RCOF)
      RMAG1=SQRT(R**2+B**2)
      THETA=ATAN(B/R)
      THETA=THETA*180/PI
      WRITE(13,299) X,RMAG
299   FORMAT (2X,F4.2,4X,F6.3)
      WRITE (6,300) X,RMAG,THETA,RZT,BZT,R
300   FORMAT (2X,F5.2,4X,F6.3,3X,F6.1,2X,E10.4,2X,E13.4,2X,
     1 E11.4,2X,E12.4/)
1000  CONTINUE
```

```
C       ------------------------------------------------------------
C       CLOSING THE FILE FOR CALCULATED DATA
C       ------------------------------------------------------------
        CLOSE(UNIT=13)
        STOP
        END
```

```
C       ********************************************************
C       *                                                      *
C       * THE PROGRAM TO PLOT MOD (K) VERSUS R1/RT USING THE *
C       * THE FILE DATA1.DAT CREATED BY THE PREVIOUS PROGRAM *
C       *                                                      *
C       ********************************************************

        DIMENSION X(1000),Y(1000)

C       ------------------------------------------------------
C       READING THE DATA FROM THE FILE DATA1.DAT
C       ------------------------------------------------------
        OPEN (UNIT=13,NAME='DATA1.DAT',TYPE='OLD')
        DO 10 I=1,100,1
        READ(13,100) X(I),Y(I)
100     FORMAT (2X,F4.2,4X,F6.3)
10      CONTINUE
        CLOSE(UNIT=13)

C       ------------------------------------------------------
C       PLOTTING THE DATA
C       ------------------------------------------------------
        CALL INIPLT(91,15.80,9.30)
        CALL WINDOW(3.0,9.0,2.0,9.0)
        CALL SCALE(0.,1.,0.,1.)
        CALL AXIS(0.2,0.2,'R1/RT',5,3,1,
        1 'MOD(K)',6,3,1)
        CALL LINE(X,Y,100,1,1,1,0)
        CALL ENDPLT

        STOP
        END
```